A computer based feasibility analysis of assessing arterial flow using pulsatility indices

by

Gerold Porenta

A Thesis Submitted to the
Graduate Faculty in Partial Fulfillment of the
Requirements for the Degree of
MASTER OF SCIENCE

Major: Biomedical Engineering

Iowa State University
Ames, Iowa

1982

TABLE OF CONTENTS

INTRODUCTION

In 1978, cardiovascular diseases accounted for 51.3% of all deaths in the United States (U.S. Department of Health and Human Services, 1980, p. 26), and to date they still pose the country's most serious health problem. The direct economic cost of illness for these diseases, that touch the life of virtually every American, amounted to 50 billion dollars in 1975 (U.S. Department of Health and Human Services, 1980, p. 33). Consequently, a major research effort has been directed towards the study of various forms of cardiovascular disease, such as atherosclerosis, cerebrovascular disease, coronary heart disease, and peripheral vascular disease. As a result, important research advances have contributed to a significant decrease in the cardiovascular death rate.

Arterial diseases are the subject of many investigations, as they are closely related to many other cardiovascular diseases. For example, the partial occlusion of a coronary artery can reduce the blood supply to the heart and lead to a myocardial infarct. A constriction of arteries supplying the brain with blood can result in a cerebral accident (stroke). Frequently, the narrowing of an arterial lumen (stenosis) causes a reduction of blood supply, but the process of the initiation and development of a stenosis is not completely understood. Much research is still in progress to advance the basic knowledge of cardiovascular diseases and to generate the most effective methods of clinical management and prevention.

Identification of risk factors has made possible an improvement of preventive actions over the past years. It appears that the public has become more aware of known cardiovascular risk factors and has adjusted behavior and lifestyle to reduce a number of risks such as the use of tobacco products and the consumption of high saturated fat-high cholesterol foods (U.S. Department of Health, Education, and Welfare, 1979, p. 2). Many aspects of the etiology of cardiovascular diseases, however, remain unknown, so that the implementation of a comprehensive and effective prevention program has been impossible to achieve so far.

Once a disease develops, successful therapy and cure often depend on an early and accurate diagnosis, not yet available for many cardiovascular diseases. Peripheral arterial diseases, which frequently do not exhibit clinical symptoms during the early stages, can remain undetected until more than 90% of the artery's lumen is occluded. At this late stage in the disease process the treatment is usually a surgical procedure, as compared to pharmacological treatment that could be used if the disease were diagnosed during the early stages. Today several diagnostic techniques are available, differing in two usually mutually exclusive aspects: efficacy and patient safety.

Arteriography, an invasive diagnostic technique, is generally considered to be more reliable than various noninvasive methods, but has a disadvantage since it involves a surgical procedure with an associated risk. Ultrasonic techniques, on the other hand, are noninvasive and can be used safely on a regular basis for routine screening of arteries, or in cases where arteriography would impose too high a risk for a

particular patient.

One diagnostic method utilizing ultrasound is based on the changes in the flow waveform that occur in diseased arteries. A pulsatility index, commonly defined as the ratio of the peak to peak velocity excursion to the mean velocity, is measured distal and proximal to the obstruction. The ratio of these two indices, called the inverse damping factor, or simply the magnitude of a given pulsatility index can presumably provide some indication of the presence of a pathological situation. This method has been used successfully in clinical situations, but a detailed analysis of the effect of various parameters such as taper and branching of arteries, measurement site, and blood viscosity on the pulsatility index has not yet been accomplished.

The purpose of this thesis is to develop a computer model of the human femoral artery and to use this model to (1) study the influence of various flow situations on generalized pulsatility indices and their corresponding inverse damping factors, and (2) investigate the feasibility of using these indices to predict the presence of a stenosed arterial segment.

In the literature review, I will (1) summarize different approaches taken in modeling arterial blood flow, (2) comment on the instrumentation available to measure blood flow in arteries, and (3) provide information on clinical applications which utilize pulsatility indices to detect abnormal flow situations. I will then present the basic equations of the theoretical model, explain the numerical procedure used to implement the model on a digital computer, and define

the pulsatility indices investigated in this study. The chapter on the physiological model will contain a description of geometry and properties of the human femoral artery and the values of system parameters. A discussion of results followed by a summary will conclude this thesis.

LITERATURE REVIEW

The following literature review is not meant to be comprehensive, as the literature on the three topics presented is so extensive that it would be far beyond the scope of this thesis to provide a complete review. Rather I will present the basic equations used in cardiovascular modeling, establish a frame of reference relating my model to its predecessors, and focus mainly on publications stressing an interrelation between modeling and clinical situations.

Models of Blood Flow in Arteries

Most of the model studies are based on three types of equations: the Navier-Stokes equation, the continuity equation, and an equation of state. Therefore, this review first provides a general discussion of these equations followed by a presentation of different applications appearing in the literature.

For more than 2000 years, blood flow in arteries has been a major point of research for many investigators with very different professional origins. But progress was very slow, and many functional features of the arterial system were still unknown in the 16th century when the classical Galenical teaching that blood was created in the liver and absorbed by the tissues to which it was conveyed with oscillatory motion mainly in the veins prevailed (McDonald, 1974, p. 4).

Essential discoveries did not come about until the 19th century when experiments were conducted more meticulously and mechanical principles were applied to cardiovascular flow situations. Using

theoretical considerations, Navier and Stokes derived an equation describing both steady and unsteady laminar flow of a Newtonian fluid. In formal mathematical terms, the Navier-Stokes equation can be written as:

$$\frac{\partial q}{\partial t} + (q.\nabla)q + \frac{1}{\rho}\nabla p - B - \frac{\mu}{\rho}\nabla^2 q = 0 \qquad (1)$$

where q is the flow vector, p the pressure, ρ the fluid density, μ the fluid viscosity, and B an external body force vector. This nonlinear partial differential equation, capable of describing very general flow situations, still defies an analytical solution in its most general form, more than 130 years after the first publication.

Another basic law in fluid mechanics is the continuity equation stating that fluid mass flowing through a control volume cannot be lost or transformed within the control volume, or in other words: mass flowing into a control volume must be balanced by the mass flowing out of it. The mathematical notation is given by

$$\nabla.q = 0 \qquad (2)$$

If applied to laminar flow of an incompressible fluid in a tube with rigid walls, the continuity equation indicates that the volume rate of flow is independent of position and therefore changes with time uniformly along the tube.

Blood flow in arteries can be simulated by assuming that (1) blood is an incompressible Newtonian fluid (generally considered to be a good assumption), and (2) arteries behave like linearly elastic tubes. For this special case, Womersley (1957) used the continuity equation to simplify the Navier-Stokes equation and obtained an analytical solution

for the flow problem. The resulting velocity profiles provide an approximation to pulsatile blood flow and correctly indicate that flow reversal (arterial flow from the periphery to the heart) can occur during the cardiac cycle, a finding well documented by in vivo studies.

Womersley's solution cannot be written in terms of explicit functions; it requires that the driving pressure be specified as a Fourier series, and each term in the Fourier series yields a corresponding flow term containing Bessel functions. That makes the solution somewhat awkward to work with. Nevertheless, Womersley's work is one of the milestones in modeling blood flow in arteries and has provided the foundation for an improved understanding of processes in the cardiovascular system. Shortly after Womersley published his research, analog and digital computers became more widely available, and many investigators took advantage of these new tools giving rise to a new branch of cardiovascular modeling presented later in this section.

A different approach to modeling originated from the science of material properties, which started in the first half of the 19th century when Thomas Young the famous biophysicist did work on the nature of elasticity. He was particularly interested in the relation between the elastic properties of arteries and the velocity of propagation of the arterial pulse. A similar problem is to find a relationship between the cross sectional area of an artery and its distending pressure. An equation of this kind, relating area and pressure, is usually referred to as an equation of state and can be obtained by both theoretical and experimental means.

Experimental studies (Roach and Burton, 1959; Boughner and Roach, 1971) relate the circumferential tension T and the percent increase in circumference of an artery. With the use of Laplace's law

$$T = pR$$

where p is the distending pressure and R the arterial radius, the tension strain curves can then be rewritten in terms of area and pressure if the value for the radius of the unstrained artery is known.

A theoretical analysis can deduce an equation of state from mechanical principles valid for thin walled vessels. Depending on the assumptions made during the derivation, different results will be obtained. Streeter et al. (1963) assumed the vessel to have a constant volume per unit length and the vessel material to be incompressible (Poisson's ratio = 0.5) and presented an equation of state in the following form:

$$A(p,x) = A(p_0,x)(1-d_0(p-p_0)/Eh_0)^{-1} \qquad (3)$$

where A(p,x) is the area as a function of pressure p and arterial length x, E is the modulus of elasticity, and d_0, h_0 are the values of vessel diameter and thickness at a reference pressure p_0. For clinical application, this equation is of limited value since equipment to measure the modulus of elasticity in vivo is not yet available.

Equation (3) can be modified by introducing a new parameter, which is clinically accessible: the pressure pulse wave velocity a_0. A simple and very useful formula for a_0 is the famous Moens-Korteweg equation

$$a_0 = (Eh_0/\rho d_0)^{0.5} \tag{4}$$

which originated from work on wave propagation in the last century. The Moens-Korteweg equation in a strict sense is valid only for nonviscous fluids, but it does provide a good approximation for blood flow. A substitution of equation (4) into equation (3) yields

$$A(p,x) = A(p_0,x)(1-(p-p_0)/\rho a_0^2)^{-1} \tag{5}$$

leaving only two parameters, the fluid density and the pulse wave velocity.

Another parameter easily obtainable in clinical situations is a pressure strain modulus E_p defined as $E_p = (R/\Delta R)\Delta p$. Mozersky et al. (1972) transcutaneously measured E_p on patients classified in three different age groups and found an increase of E_p with age. They also observed large variations within the age groups. By integrating the definition of E_p, an equation of state in the form

$$A(p,x) = A(p_0,x)e^{2(p-p_0)/E_p} \tag{6}$$

can be obtained. Equations (3), (5), and (6) all relate the distending pressure and the cross sectional area and therefore represent different realizations of an equation of state. As a common feature, they only concentrate on the elastic behavior of arterial walls and neglect any viscoelastic behavior which would give rise to the possibility of phase differences between pressure and area. For many modeling situations, departures from elastic behavior are not of prime interest, in which case the elastic theory yields adequate results.

Efforts to model one dimensional arterial flow on computers started two decades ago on analog computers where simplified and linearized equations were implemented. As more sophisticated algorithms became available to solve partial differential equations on digital computers, the research emphasis shifted towards digital computers, partly because nonlinearities can be included with relative ease.

Snyder et al. (1968) set up a linear model of the systemic arterial tree on an analog computer and obtained results that agree with physiological data such as distal delay and peaking of pressure pulse waves. Moreover, several clinical parameters such as cardiac output and cardiac work were investigated with respect to variations in the heart rate.

Westerhof et al. (1969) used a linear model to build an electric analogy of the total human systemic arterial tree. They discuss several concepts of vascular impedance and wave travel and prove that a simple aortic model consisting of a single tube with only one distal reflection site at its end does not accurately represent the physiological situation. The peripheral peaking of the pressure pulse is attributed to reflections for lower harmonics at the peripheral beds simulated by a lumped pure resistance. Westerhof et al. neglect viscoelastic behavior and, for clinical comparisons, simulate effects of essential and old age hypertension.

Schaaf and Abbrecht (1972) compare linear and nonlinear models on a digital computer and conclude that the higher fidelity obtained with nonlinear models is due to the effects of vessel taper and the

convective acceleration term in the Navier-Stokes equation. In more detail, Schaaf and Abbrecht attribute the main differences to the nonlinear effects of finite wall displacements and only small influences to the terms in the Navier-Stokes equations corresponding to convective acceleration and fluid friction. The influence of the peripheral beds are accounted for by including a distal lumped resistance.

Wemple and Mockros (1972) used the methods of characteristics to implement a nonlinear model on a digital computer by including convective acceleration and fluid friction for steady and first harmonic sinusoidal flow in the Navier-Stokes equation and by allowing the modulus of elasticity in the equation of state to be a function of cross sectional area (elastic taper). Simulation of the peripheral beds in this model is more elaborate than in the models presented above, as it provides for both resistive and compliant components. Like Snyder et al. (1968), Westerhof et al. (1969), and Schaaf and Abbrecht (1972), Wemple and Mockros concentrate on the behavior of the pressure pulse wave and try to determine its governing factors. From their results, Wemple and Mockros conclude that reflections at the distal end are mainly responsible for pulse wave amplification, whereas geometrical taper does not exhibit a major influence. Wemple and Mockros also suggest that elastic taper and nonlinearities in the wall elasticity do not significally alter pressure and flow profiles. For low frequencies, their nonlinear model deviates only slightly from the linear model.

Raines et al. (1974) limit their model based on a finite-difference numerical technique to the human femoral artery and try to stay very

close to the in vivo situation. In assessing the various effects of parameter variations on almost exclusivly the pressure waveform, they retain the nonlinearities in the governing equations. Many different physiological conditions are simulated during the sensitivity analysis. Networks of a resistance in series with a parallel combination of a resistance and a compliance account for the effects of two branches and the arterial tree distal to the popliteal artery. The terminating networks can be physiologically interpreted by attributing the effects of the first resistance to the flow resistance located in the arterioles and the effects of the parallel combination to the influences of the capillary bed. From the sensitivity analysis, Raines et al. deduce that the pressure waveform is only moderately affected by the convective acceleration, blood viscosity, and branching, but that vessel elasticity and distal reflections strongly determine the behavior of the pressure pulse. These results are in good agreement with Schaaf and Abbrecht (1972) and Wemple and Mockros (1972).

Overall, the basic model of the human femoral artery as presented by Raines et al. (1974) includes all the main features known to determine flow and pressure waveforms, and at the same time provides a model geometry and a set of parameters that simulates rather closely the in vivo situation. Therefore, the control case of Raines et al. will be adopted as the basis for the model in this thesis.

Diagnostic Methods for Measuring Arterial Flow

The most common diagnostic method is arteriography, an invasive method where a radioactive tracer material is injected into the artery and x-ray pictures are taken providing information about the presence of a constriction. This method is considered to be the most reliable diagnostic technique; however, it is relatively time consuming, expensive, cannot be used repeatedly for routine screening and followup examinations, is associated with a certain degree of morbidity and mortality, and may indicate less arterial obstruction than is present (Lee et al., 1980). In an attempt to overcome these difficulties, noninvasive techniques have been developed based on the abnormal flow characteristics that develop in stenosed arteries.

Electromagnetic flowmeters, in the past used only on exposed arteries during surgery, now are used noninvasively by creating the magnetic field exterior to the body. Lee et al. (1980) reported on the successful application of a noninvasive calibrated electromagnetic flowmeter in assessing arterial peripheral flow.

Ultrasonic devices are the most frequently used noninvasive diagnostic instruments in a clinical environment. One ultrasonic technique produces scans of arteries by colouring images according to the peak velocity at each point in the artery. Abnormalities are identified by change of flow velocity rather than direct visualization of vessel narrowing. Another device displays all frequencies occurring in the Doppler signal versus time. For smooth blood flow, the Doppler energy is concentrated in a narrow frequency spectrum, whereas for

turbulent flow, energy is spread over a wider frequency range. The physician then deduces from the distribution of energy the flow situation.

Ultrasonic flowmeters which provide a measurement of the flow waveform at one specific point of the artery during a cardiac cycle have been used extensively to assess peripheral arterial flow (Gosling et al., 1971, Harris et al., 1974, Johnston et al., 1978, Baird et al., 1979). Two techniques, the continuous wave Doppler flowmeter (CW Doppler) and the pulsed Doppler flowmeter, differ in the way the flow waveform is obtained. The CW Doppler measures velocity components over the total arterial cross section, which are used to generate a representative wave sample. Johnston et al. (1977) point out problems associated with the use of CW Dopplers and present solutions to overcome these problems. Pulsed Doppler flowmeters concentrate on a restricted area of the total arterial lumen, and depending on the size of an artery, can be used to obtain flow waveforms at several sites between the arterial wall and the arterial center. Baird et al. (1979) measured flow waveforms with a 30 channel pulsed Doppler flowmeter at 4 points across the section of the femoral artery.

At the present time, both CW and pulsed Doppler flowmeters are difficult to calibrate accurately, and their output waveforms are usually graded by qualitative means to provide a comparison of data from different patients.

Noninvasive Assessment of Arterial Flow

All of the following methods for assessing arterial flow are based on the evaluation of flow waveforms obtained with uncalibrated ultrasonic equipment.

Arterial obstructions cannot be detected by ultrasonic methods unless they cause changes in the flow behavior. Often, stenoses are thought to dampen the flow waveform and reduce the pulsatility of blood flow along the artery. During the past ten years, several methods have been introduced to associate a pulsatility index with flow waveforms and to deduce the flow situation from variations of the pulsatility index along the artery. Because of easy accessibility, the arteries in the human legs have served as a benchmark for the different methods.

Gosling et al. (1971) were the first to use a pulsatility index (PI) defined as the total oscillatory energy in the flow velocity waveform divided by the energy of the mean forward flow velocity during a cardiac cycle. By looking at the variation of the PI from the abdominal aorta to the tibial arteries, Gosling et al. could arrive at a quantitative comparison of the arterial pathway capabilities of different patients.

Woodcock et al. (1972) introduced the damping factor (DF) as the ratio of proximal and distal measured PIs and tried to relate the DF with pressure drop and flow. Their results indicate that the DF method is in agreement with other methods (arm/calf pressure difference, strain-gauge plethysmography) and could be useful in the assessment of arterial flow. However, Woodcock et al. did not present a method that

could quantitatively correlate the DF with the degree of arterial obstruction.

Harris et al. (1974) studied the relationship between an assessment using the pulsatility index and angiography in occlusive arterial diseases in the human limbs. Their work led to the conclusion that assessments of disease by the 2 methods correlate, but that the ultrasound method could incorrectly disclose a severe disease which was not apparent in the angiography.

According to the original definition of the PI, its evaluation requires the flow waveform to be presented in Fourier coefficients, thereby making necessary a conversion of flow data from the time to the frequency domain. Thus, Gosling and King (1974) trying to overcome this computational disadvantage defined a pulsatility index as the ratio of peak to peak flow excursion to the mean flow. This PI with the same information content as the previous one (Gosling and King, 1974; Johnston et al., 1978) is easier to evaluate. Subsequent studies (Johnston and Taraschuk, 1976; Johnston et al., 1978; Baird et al., 1979, Evans et al., 1980) made use of this new definition of the PI.

Johnston and Taraschuk (1976) compared the PI method with graded arteriograms and ankle systolic pressure measurements. Their results suggest that the PI method is capable of detecting clinically significant stenoses (more than 50% area obstruction) and may be sensitive enough to detect lesions graded by arteriograms as less than 50% stenosis. However, the authors recommend that a precise sensitivity analysis, not included in their study, be carried out on the

investigated patient group.

In a later study, Johnston et al. (1978) comment on problems associated with the CW Doppler device hardware, present an improved system, and demonstrate that clinically significant peripheral arterial occlusive disease can be quantified and regionally localized with the PI method. Also, the authors prefer to use the inverse damping factor (IDF) because like most clinical measurement indices it decreases with increasing disease state. Moreover, the IDF (with a fixed proximal PI and a varying distal PI) plotted against arterial tube length shows the behavior of a normalized pulsatility index along the artery in a proportionate fashion (independent variable in the numerator of the ratio) as opposed to the inverse proportional plot of the DF along the artery. For most people, proportional curves are easier to interpret. For these two reasons, I chose to investigate the behavior of the IDF instead of the DF which is more common in the literature.

Baird et al. (1979) working with a 30-channel pulsed Doppler flowmeter scanned the profunda branch of human femoral arteries and found that a stenosis of more than 50% was invariably associated with a IDF of less than 0.67. For normal limbs, the IDF was always greater than 0.71.

Evans et al. (1980) conducted an analysis of the relationship between ultrasonic PI and proximal arterial stenosis in a canine model. After implanting stenoses of varying lengths and cross sectional areas, the authors were able to show that the reduction of the PI (= IDF of less than 1.0) correlates broadly with the stenosis severity, but that

at the same time all but the tightest stenoses exhibit a wide scatter in the results, an effect attributed to the influence of peripheral resistance. Therefore, the dependency of the PI on the peripheral resistance is much more marked in the case of mild stenosis, whereas tight stenoses always result in a low PI. In the animal model, only stenoses greater than 86% produced an PI low enough to be diagnostic of inadequate flow.

The study of Evans et al. (1980) shows clearly that the diagnostic value of the PI method depends significantly on an accurate knowledge of its sensitivity to parameter variations. A detailed sensitivity analysis, however, cannot be performed in animal models. Therefore, I studied the sensitivity of the PI method on a computer model and investigated the feasibility of using PI and IDF to assess arterial flow.

THEORETICAL MODEL

Governing Equations

Three equations describing general fluid flow situations were presented in the previous chapter: momentum equation, continuity equation, and an equation of state. The three independent variables in these equations are the three dimensional flow vector $q(x,t)$, the pressure $p(x,t)$, and the cross sectional area $A(p,t)$. For the purpose of this study, all three equations were modified to obtain a description of arterial blood flow that can be treated numerically with relative ease.

The Navier-Stokes equations can be reduced to an equation of the form

$$A\frac{\partial Q}{\partial t} + 2Q\frac{\partial Q}{\partial x} - (Q^2/A)\frac{\partial A}{\partial x} + (A^2/\rho)\frac{\partial p}{\partial x} + \frac{8\pi\mu}{\rho}Q = 0 \qquad (7)$$

by integrating equation (1) over the arterial cross section and making the following assumptions:

1. Arterial flow is axisymmetric.
2. The blood layer adjacent to the arterial wall follows the wall motion ('no slip' condition).
3. The pressure is uniform across the arterial cross section.
4. The wall stress for arterial flow can be approximated by the wall shear stress for steady flow.
5. The second derivative of the axial flow component with respect to axial location is small compared to other terms in the Navier-Stokes equations and can be neglected.

The second and third term in equation (7) are the convective acceleration terms, and the last term is the fluid friction term. In the following, equation (7) will be referred to as momentum equation.

The continuity equation can also be integrated over the arterial cross section. By neglecting flow through the arterial wall (seepage) and using the first two assumptions from above, the following equation can be obtained:

$$\frac{\partial Q}{\partial x} + \frac{\partial A}{\partial t} = 0 \tag{8}$$

The two forms of an equation of state given in equations (5) and (6) include a type of nonlinearity that is not well-suited for the numerical algorithm of finite elements used in this study. Therefore, I chose to work with an approximation in the form of a second order polynomial

$$A(p,x) = A(p_0,x)(1 + C_0^a(p-p_0) + C_1^a(p-p_0)^2) \tag{9}$$

The coefficients of the polynomial C_0^a and C_1^a can be found by rewriting equation (5) as a geometrical series or expanding equation (6) into a Taylor series and neglecting terms of higher order. Alternatively, fitting equation (9) to pressure area curves from experimental studies also yields values for the coefficients. In any case, the resulting approximation has to be examined carefully with respect to accuracy. For example, the validity of equation (5) in a rigorous sense is assured only for small pressure variations around a reference pressure p_0. An approximation of the equation of state based on equation (5) will therefore not be equally precise over the full range of arterial

pressure where the mean arterial pressure is taken as p_0. Compared to the assumptions included in the derivation of equations (7) and (8), the approximation of the equation of state by equation (9) probably introduces the most significant deviation from the physiological situation.

To obtain two equations containing partial derivatives with respect to only two independent variables, equation (9) can be used to eliminate the area derivative in equation (8). After the substitution, the continuity equation has the form

$$\frac{\partial Q}{\partial x} + A(p_0,x)\left(C_0\frac{\partial p}{\partial t} + C_1 p\frac{\partial p}{\partial t}\right) = 0 \qquad (10)$$

where

$$C_0 = C_0^a - 2p_0C_1^a$$

$$C_1 = 2C_1^a$$

Equations (7) and (10) constitute the governing equations of blood flow in unobstructed arteries without branches.

To simulate an arterial section that includes a branch diverting from the main stem, two equations are needed to replace equations (7) and (10). The effects caused by a branch are usually lumped into equations containing parameters that account only for the overall hemodynamic behavior and do not provide a detailed flow description such as equations (7) or (10). As a good approximation, the small pressure drop across the branch location can be neglected. Thus,

$$\frac{\partial p}{\partial x} = 0 \qquad (11)$$

takes the place of the momentum equation. The form of the second equation which includes the effect of branch flow depends on the model adopted for the peripheral beds. In many studies, this is chosen to be a pure lumped resistance. However, Raines et al. (1974) stated that the compliant contribution of the peripheral beds plays a role in determining the distal pulse wave form; consequently they used a network which includes a resistance R_1 in series with the parallel combination of a resistance R_2 and a compliant element C to simulate peripheral beds. I also considered this constellation to be more realistic and incorporated it into my model. With the assumption that the venous pressure is zero, the equation for the branch flow B is

$$C\frac{dp}{dt} - R_1C\frac{dB}{dt} + p/R_2 - (1+R_1/R_2)B = 0 \qquad (12)$$

From the continuity principle, it follows that B is the difference between the flow before and after the branching point in the main arterial stem. At the distal end, the flow rate in the main artery obeys the same equation as B in equation (12).

In addition to unobstructed arteries, stenosed arteries will also be simulated in this study. Thus, two more equations are needed that involve the pressure drop across the stenosis and the corresponding volume rate of flow. If the stenosed arterial section is considered to be noncompliant, the continuity equation (8) reduces to

$$\frac{\partial Q}{\partial x} = 0 \qquad (13)$$

which gives the first of two required equations. The second equation is taken from Young and Tsai (1973) who studied unsteady flow through rigid

tubes with different types of obstructions and combined theoretical and experimental data to develop the relationship

$$A_0\frac{\Delta p}{\rho L} = (K_v)\frac{\mu}{DL\rho}Q + (K_t/2A_0)[A_0/A_1-1]^2Q|Q| + (K_u)\frac{\partial Q}{\partial t} \qquad (14)$$

and

$$K_v = 32[(0.83L + 1.64D_1)/D](A_0/A_1)^2$$

where Δp is the pressure drop across the stenosis, A_0, D and A_1, D_1 are the areas and diameters of the unobstructed and obstructed arterial lumen, respectively, and L is the length of the stenosis. In my model, K_t and K_u were assigned the values 1.5 and 1.2. These empirical values correspond to stenoses having the shape of blunt ended, hollowed plugs. A derivation of this equation and a discussion of various hemodynamic factors pertaining to blood flow in stenosed arteries are given in Young (1979).

In summary, a pair of equations containing the partial derivatives of flow and pressure with respect to time and position have been presented for three different model situations: unobstructed artery without a branch, unobstructed artery including a branch, and obstructed artery. Given a description of the model geometry and a specification of proper boundary values, a numerical solution to these equations will yield values of pressure and flow at selected points along the artery.

Numerical Procedure

The governing equations of the model include nonlinear terms and thus cannot be solved analytically. Instead, numerical methods that can be implemented on a digital computer have to be used to provide an approximate solution. Most numerical methods are based on a discretization process where the derivative terms in the partial differential equations are replaced with algebraic expressions. If the discretization process is carried out in accordance with certain restrictions, the solution to the system of algebraic equations represents an accurate approximation to the analytical solution of the partial differential equations.

In my model, several sets of partial differential equations interact with each other, corresponding to the differences in arterial sections (without a branch, with a branch, and with a stenosis). Inhomogenous model geometry like this can be treated with relative ease by the numerical method of finite elements. Rooz (1980) gives a detailed step by step description of applying the finite element method using the Galerkin method to equations simulating blood flow. Overall, this method is not only well-suited to discretize flow equations, but it is also relatively easy to implement. Therefore, I extended his approach to the more general equations of this study.

In the Galerkin method, the domain of the independent variables, location and time, is divided into rectangular elements with four nodes situated at the corners of an element. The dependent variables, pressure and flow, are assumed to be of the form

$$Q(x,t) = [N(x,t)]\{q\} \tag{15}$$

and

$$p(x,t) = [N(x,t)]\{p\} \tag{16}$$

where {q} and {p} are four dimensional column vectors consisting of the unknown flow and pressure values at the four nodes, and [N(x,t)] is a four dimensional row vector of the shape functions N_i. The N_i are chosen so that they assume the value 1 at node i and 0 at the three other nodes. After substitution of equations (15) and (16) into a pair of corresponding differential equations such as (7) and (10), the resulting differential forms are multiplied by each of the four shape functions and integrated over the element area. The result is a set of 8 homogeneous algebraic equations for the 8 unknown values of pressures {p} and flow rates {q} at the four element nodes.

According to the underlying geometry, the element equations are then inserted into a global matrix using the direct stiffness assemblage with respect to arterial position. This yields a homogeneous system of algebraic equations

$$A'\{\delta\} + B'\{\delta\} = 0 \tag{17}$$

where A' and B' are 4(n+1) dimensional matrices with A' independent and B' dependent on δ. The quantity δ is a 4(n+1) dimensional row vector containing the unknown values of pressure and flow at the nodes of n elements representing a discretization of the flow problem at times τ and $\tau+\Delta t$. Note that system (17) is singular unless proper boundary conditions are inserted.

The complexity of system (17) can be reduced by assuming that the

values of pressure and flow at time τ are already known and performing the appropriate substitution in system (17). The number of unknown values reduces to 2(n+1) and half of the equations in system (17) can be discarded. A review of the Galerkin process reveals that this reduction can actually be accomplished during the derivation of the element equations by taking only two of four shape functions as multiplication factors prior to the integration step. Appendix 1 contains the element equations for the three different pairs of differential equations in the reduced form. After reduction, (17) can be written as

$$A\{\delta\} + B\{\delta\} = \{f\} \tag{18}$$

where the dimension of A, B, and $\{\delta\}$ is now 2(n+1), and $\{f\}$ consists of the terms originating from the substitution of the initial values at time τ. The reduction in dimension of system (17) brings about an increase in required time steps. For a fixed time span, system (18) has to be solved twice as often as system (17).

Contributions to matrix B which is a function of $\{p\}$ and $\{q\}$ originate from three sources: the convective acceleration term of the Navier-Stokes equation (7), the second order term in the equation of state (9), and the nonlinear term in the formula for the pressure drop across a stenosis (14). The dependency of B on values of the solution $\{\delta\}$ makes necessary the utilization of an iterative method to obtain a solution to system (18). An iteration can be defined by

$$A\{\delta_n\} + B_{n-1}\{\delta_n\} = \{f\} \tag{19}$$

where B_{n-1} is B evaluated at $\{\delta_{n-1}\}$. Equation (19) represents a linear system. For the first iteration step, the values of pressure and flow

from the previous time step serve as initial values to evaluate B_0. Iteration (19) is terminated if the relative difference of two successive iterations becomes smaller than a given tolerance or if the number of iterations exceeds a preset value. I chose 0.1% as an accuracy threshold and terminated the program execution if more than 10 iterations were required.

The computer program to solve system (18) was written in FORTRAN for implementation on a high-speed digital computer, the ITEL6. The input file contains

- a description of the flow problem geometry including specifications of the R_1, R_2, and C values for the branches and the distal end,
- flow parameters such as fluid density and fluid viscosity,
- numerical control variables such as number of time steps, number and length of elements, and required accuracy,
- the proximal boundary values represented by the pressure waveform in the form of Fourier coefficients.

The program output includes values of pressure and flow at the proximal and distal end at selected time steps, the numerical values of all general pulsatility indices along the artery as defined in the next section, and multicolored plots of selected data curves to help with the interpretation of results.

A short outline of the program procedure follows. After data input and initialization of parameters, matrix A of system (18) is assembled and permanently stored in a global array as it remains unchanged for all

following time steps. Matrix A can be made a sparse matrix with a bandwith of 7 (for the reduced system (18)) if a certain sequence in numbering the element nodes is followed. Then, initial values are arbitrarily assigned to the pressure and flow variables. The influence of these arbitrary initial conditions is eliminated in the final solution by executing the program for three successive heart cycles so that a stable solution is obtained.

Then for each time step Δt, an iteration is performed according to equation (19) until the preset accuracy requirement is achieved. Fortunately, the linear system (19), which has to be solved for each step of the iteration, consists of two band matrices with a bandwith of 7 resulting in a considerable reduction of memory space and computation time for the solution process as compared to a full size system. In my program, I used a subroutine of the LINPACK library package to perform the solution of system (19). A rough estimate for the execution time required by the subroutine SGBFA shows that execution time is a linear function of the order of the matrix and a quadratic function of the bandwith. Thus, system (19) with a bandwith of 7 is superior to system (18) with a bandwith of 15 even in computation time. A different version of this subroutine also provides an estimation of the condition number, which can be interpreted as an error amplification factor. For an element length of 0.02 m and a time step of 0.0025 s, the condition number turned out to be 42, which can be considered a good value (the optimal value would be 1).

Pulsatility and Area Indices

Originally, the pulsatility index was defined as the ratio of the oscillatory energy of the flow waveform to the energy in the steady flow component. However, at the present time the pulsatility index usually refers to the ratio of the peak to peak velocity excursion to the mean flow. In both cases, the pulsatility index represents a dimensionless parameter associated with flow that is presumably changed through the presence of arterial obstructions. Of course, dimensionless quantities can be related to waveforms in many different ways, and it is the purpose of this study to investigate whether different measures of pulsatility could provide a better diagnostic tool to discern arterial obstructions.

One alternate measure arises from the mathematical theory of functional analysis which furnishes many different possibilities to assign to functions a numeric value, called the norm of a function. With that concept in mind, I defined dimensionless L_n-norms of the flow Q as

$$L_n(Q) = \left(\frac{1}{T}\int Q^n(t)dt\right)^{1/n}/Q_m \qquad (20)$$

where Q_m is the mean flow defined as

$$Q_m = \frac{1}{T}\int Q(t)dt$$

and included the cases n=2,3,4 in my investigation.

The distribution of the area under the flow curve provides another measure of pulsatility. A 50% area index can be defined as the ratio of the areas between 50% and 100% of the maximal and minimal flowrate to

the area under the mean flow rate. Figure 1 illustrates graphically this definition. Area indices considered in this study were the 50%, 70%, 80%, and 90% area indices. For a flat and dampened waveform, the area index will be greater than for a pulsatile waveform with sharp peaks provided that the mean flow rate is equal. Thus, an inverse damping factor based on the area indices when plotted versus arterial length may also be diagnostic of flow obstructions.

In summary, the eight different general pulsatility indices considered in this study are the conventional pulsatility index, the L_2, L_3, and L_4 norms, and the 50%, 70%, 80%, and 90% area indices together with their corresponding inverse damping factors.

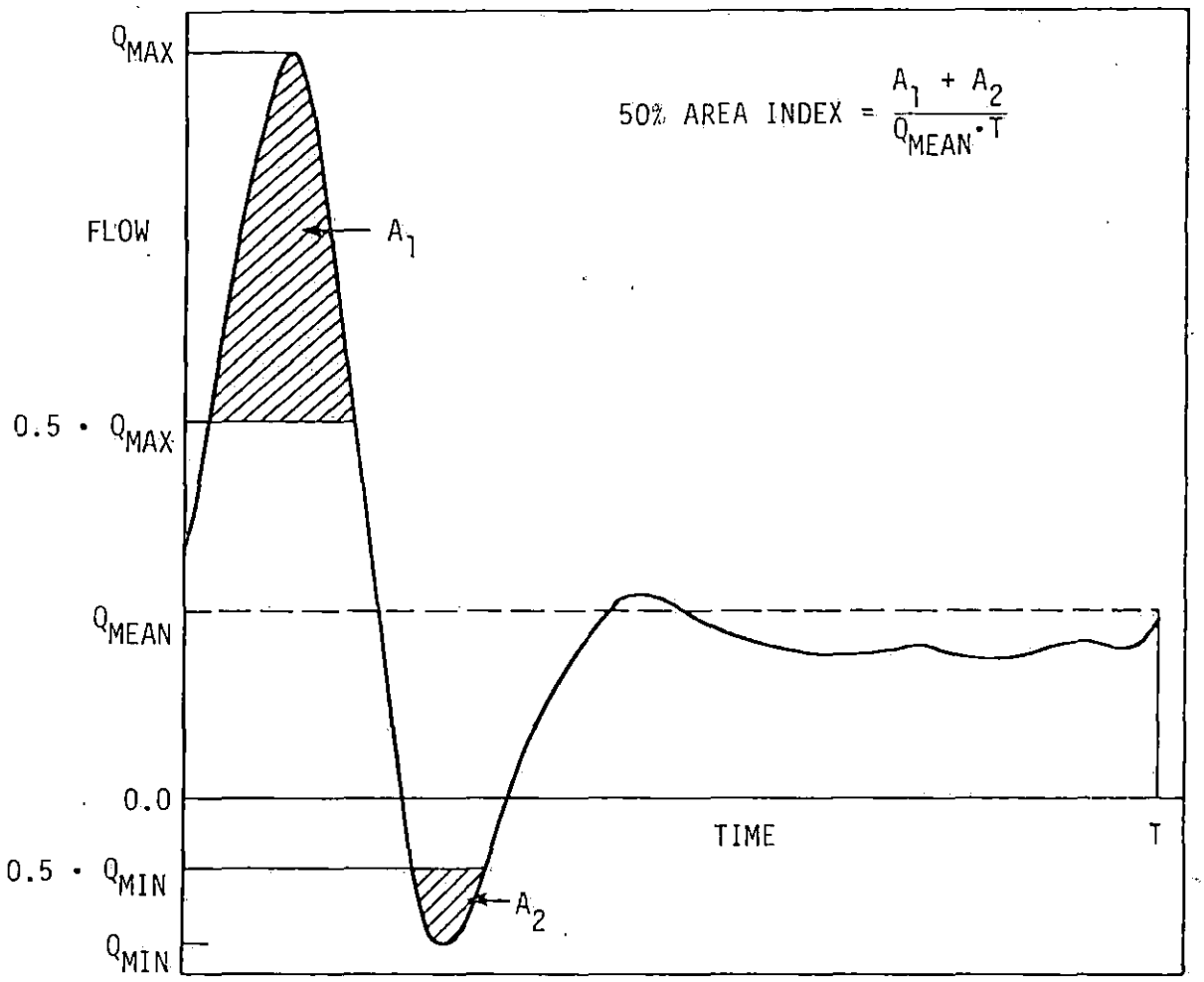

FIGURE 1. Definition of the 50% Area Index

PHYSIOLOGICAL MODEL

Raines et al. (1974) present a model of the human arterial tree from the iliac bifurcation to the point where the popliteal artery meets the tibial branches. In my study, I retained the salient features of their model, especially the model geometry, but chose a different representation of the equation of state for numerical reasons. A schematic of the model geometry is given in Figure 2.

The branches occurring in vivo along the total arterial section are lumped together into two model branches, the hypogastric artery and the profunda branch of the femoral artery. The peripheral beds of the branches and the arterial tree distal from the popliteal artery are each accounted for by a lumped model containing two flow resistances R_1, R_2 and one flow compliance C.

From measurements on arteriograms, Raines et al. (1974) obtained a relationship between the arterial area $A(p_0,x)$ at a reference pressure p_0 and the distance x from the iliac bifurcation

$$A(p_0,x) = \begin{cases} 0.505\exp(-0.192x^{0.5}) & 0 <= x <= 14 \\ 0.327\exp(-0.0206x) & 14 <= x <= 60 \end{cases} \qquad (21)$$

where x is measured in cm and A in cm^2.

Table 1 provides a summary of the system parameters in the control case. The coefficients for the equation of state were obtained by expanding (5) into a geometrical series and neglecting terms of higher than second order. The value for the blood density was assumed to be

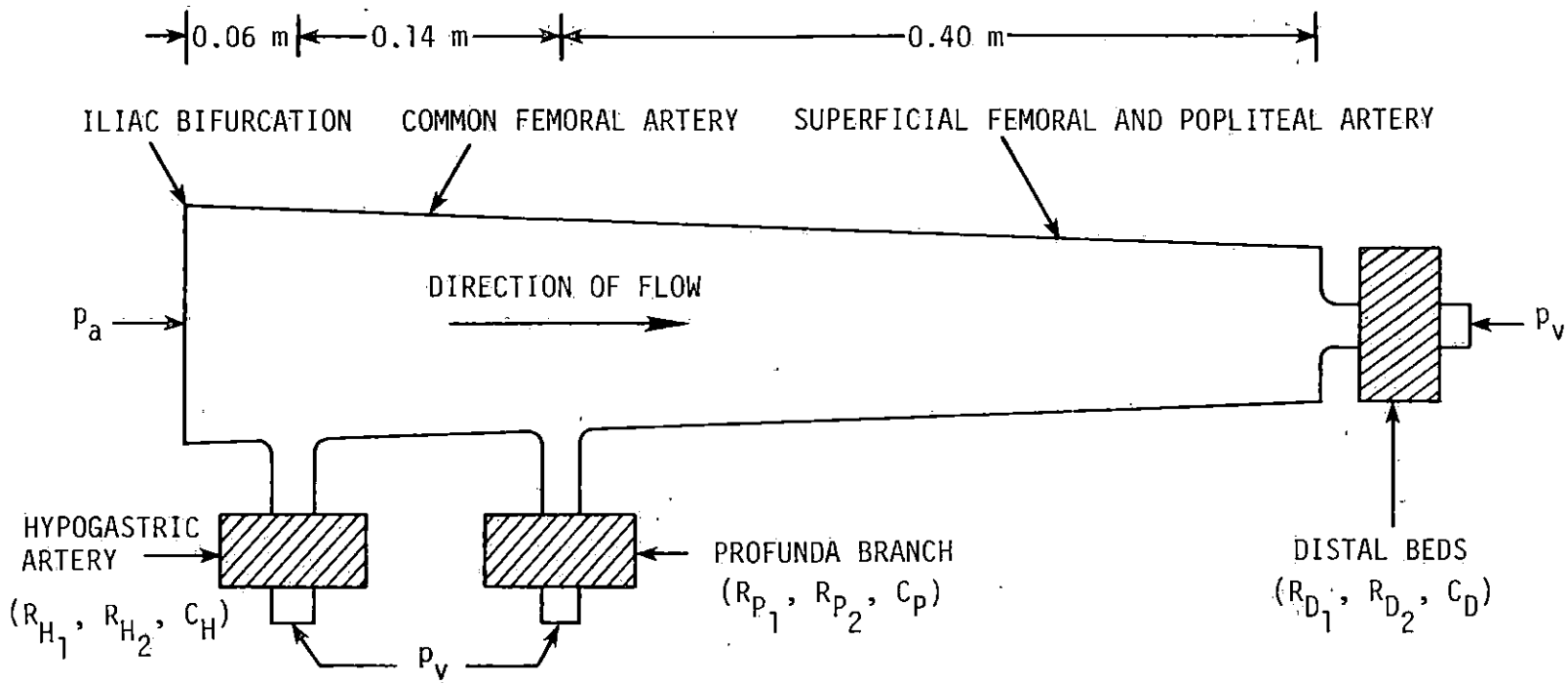

FIGURE 2. A Schematic of the Arteries in the Human Leg (p_a and p_v are the arterial and venous pressures, respectively, and (R_1, R_2, C) is a parameter triplet characterizing the corresponding peripheral bed.)

1050 kg/m^3. All other parameters are from Raines et al. (1974).

TABLE 1. Model Parameters for the Control Case

parameter description	symbol	value	units
heart rate		$0.75\ 10^{2}$	beats/min
blood density	ρ	$0.105\ 10^{4}$	kg/m^3
blood viscosity	μ	$0.45\ 10^{-2}$	Ns/m^2
pulse wave velocity	a_0	$0.104\ 10^{2}$	m/s
equation of state			
linear compliance term	C_0	$0.67\ 10^{-5}$	m^2/sN
nonlinear compliance term	C_1	$0.16\ 10^{-9}$	m^4/sN^2
hypogastric artery			
first resistance	R_{H1}	$0.43\ 10^{9}$	Ns/m^5
second resistance	R_{H2}	$0.17\ 10^{10}$	Ns/m^5
compliance	C_H	$0.15\ 10^{-9}$	m^5/N
profunda branch			
first resistance	R_{P1}	$0.85\ 10^{9}$	Ns/m^5
second resistance	R_{P2}	$0.34\ 10^{10}$	Ns/m^5
compliance	C_P	$0.75\ 10^{-10}$	m^5/N
distal end			
first resistance	R_{D1}	$0.85\ 10^{9}$	Ns/m^5
second resistance	R_{D2}	$0.34\ 10^{10}$	Ns/m^5
compliance	C_D	$0.75\ 10^{-10}$	m^5/N

To complete the model, boundary values have to be specified at the proximal end of the artery. For this purpose, I chose to use the pressure waveform since it is probably less affected than the flow

waveform by changes in the flow situations downstream from the iliac bifurcation. The proximal boundary condition in my model was unchanged for all sensitivity tests. An approximation to the pressure waveform was obtained by performing a Fourier transform on the pressure curve given in Raines et al. (1974). Only the first 7 coefficients for sine and cosine terms, as listed in Table 2, were used in the computer program to reconstruct the pressure waveform.

TABLE 2. Fourier Coefficients for the Proximal Pressure Wave

harmonics	cosine coefficient[a]	sine coefficient[a]
0	$0.1056\ 10^{5}$	0.0
1	$0.7665\ 10^{3}$	$0.2059\ 10^{4}$
2	$-0.4450\ 10^{3}$	$0.1752\ 10^{4}$
3	$-0.1246\ 10^{4}$	$0.5360\ 10^{3}$
4	$-0.6321\ 10^{3}$	$-0.3442\ 10^{3}$
5	$-0.1365\ 10^{3}$	$-0.3161\ 10^{3}$
6	$0.1211\ 10^{2}$	$-0.1285\ 10^{3}$

[a] The coefficients have as unit N/m^2.

RESULTS AND DISCUSSION

Control Case

The control case is specified by the data given in Table 1 and Figure 2. Figures 3 and 4 contain pressure and flow waveforms, respectively, at four different sites along the artery: at the proximal end, at two locations immediately following the branching points of the hypogastric artery (first branch) and the profunda artery (second branch), and at the distal end.

The pressure wave travelling along the artery shows both an amplification in the distal direction and the occurrence of a hump at the distal end, generally attributed to the effects of reflections. These findings are in good agreement with Raines et al. (1974); however, in my model the increase in the pressure wave is more marked corresponding favorably with data from physiological studies (Remington and Wood, 1956). This quantitatively different behavior is probably caused by the different form of the equation of state in my model.

The flow waveform exhibits a decrease in the distal direction as the mean flow reduces after each branch. A phase of flow reversal occurs along the total arterial section. The mean flow rates are slightly higher than those given in Raines et al. (1974).

Figure 5 shows the inverse damping factors (IDF) of the pulsatility index (PI) and of the L_2, L_3, and L_4 norms. The IDF is defined as the ratio of a distal index measurement to a proximal measurement. In the figures showing the behavior of the IDF along the artery, such as Figure

5, the proximal measurement site remains fixed at the iliac bifurcation, and the distal measurement site varies along the artery. Note in Figure 5, that the IDF of the PI remains clearly above 0.67, a value which has been correlated with arterial disease by Baird et al. (1979). Instead of the IDF, Baird et al. (1979) use the damping factor which is found to be greater than 1.5 for arteries with more than 50% stenosis. As shown in Figure 5, branching causes an increase in the IDF as the reduction in mean flow exceeds the reduction in the difference between maximal and minimal flow rates (compare the definition of the pulsatility index).

The IDFs for the area indices are depicted in Figure 6. As is the case for the IDF of the pulsatility index, the IDFs of the area indices increase at branching points and decrease slowly along the normal arterial sections. The graphs of the IDFs for all area indices are almost identical showing only small variations at the distal end which could be caused by numerical errors. At the present time, I do not have a pertinent hemodynamic interpretation for this unexpected behavior.

A linear model version, which excluded the nonlinear convective acceleration term of the momentum equation and the nonlinear term of the equation of state, shows different results. The pressure pulse wave is not amplified in the distal direction, and the hump in the pressure curve is less obvious. However, if the convective acceleration term is retained and a linear equation of state is used, both phenomena (pressure amplification and distal hump) appear regardless of whether the model geometry includes area taper or not. In the case of equal taper, a smaller arterial area causes a larger distal amplification. I

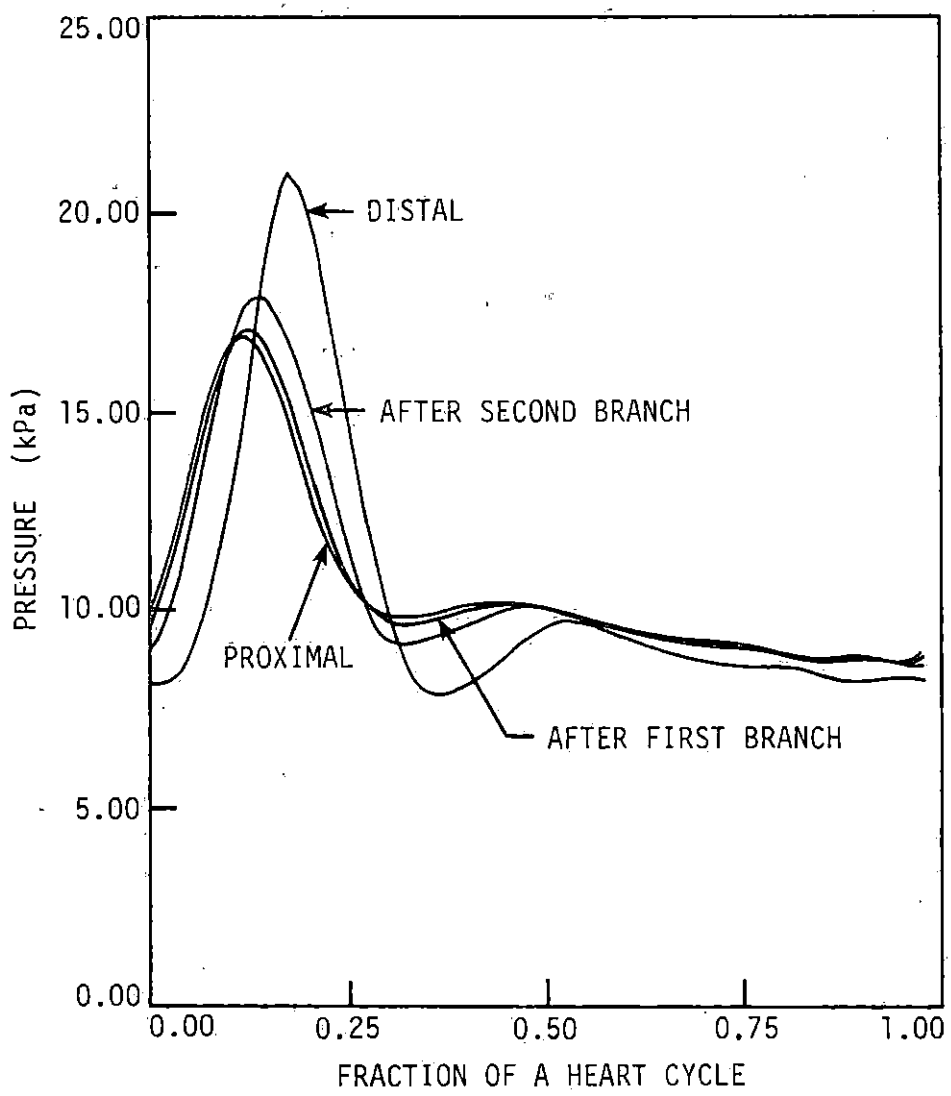

FIGURE 3. Pressure Waves along the Artery for the Control Case

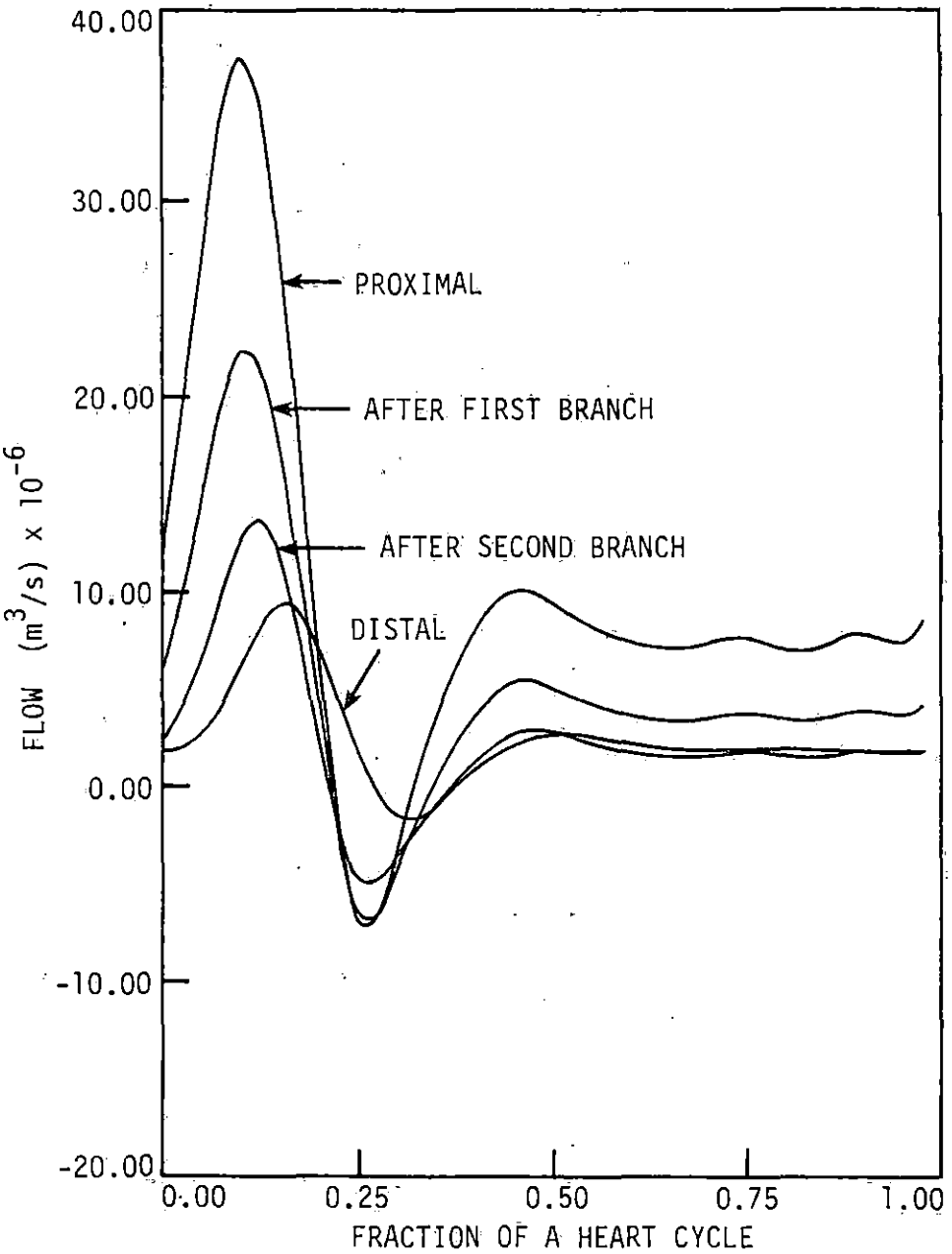

FIGURE 4. Flow Waves along the Artery for the Control Case

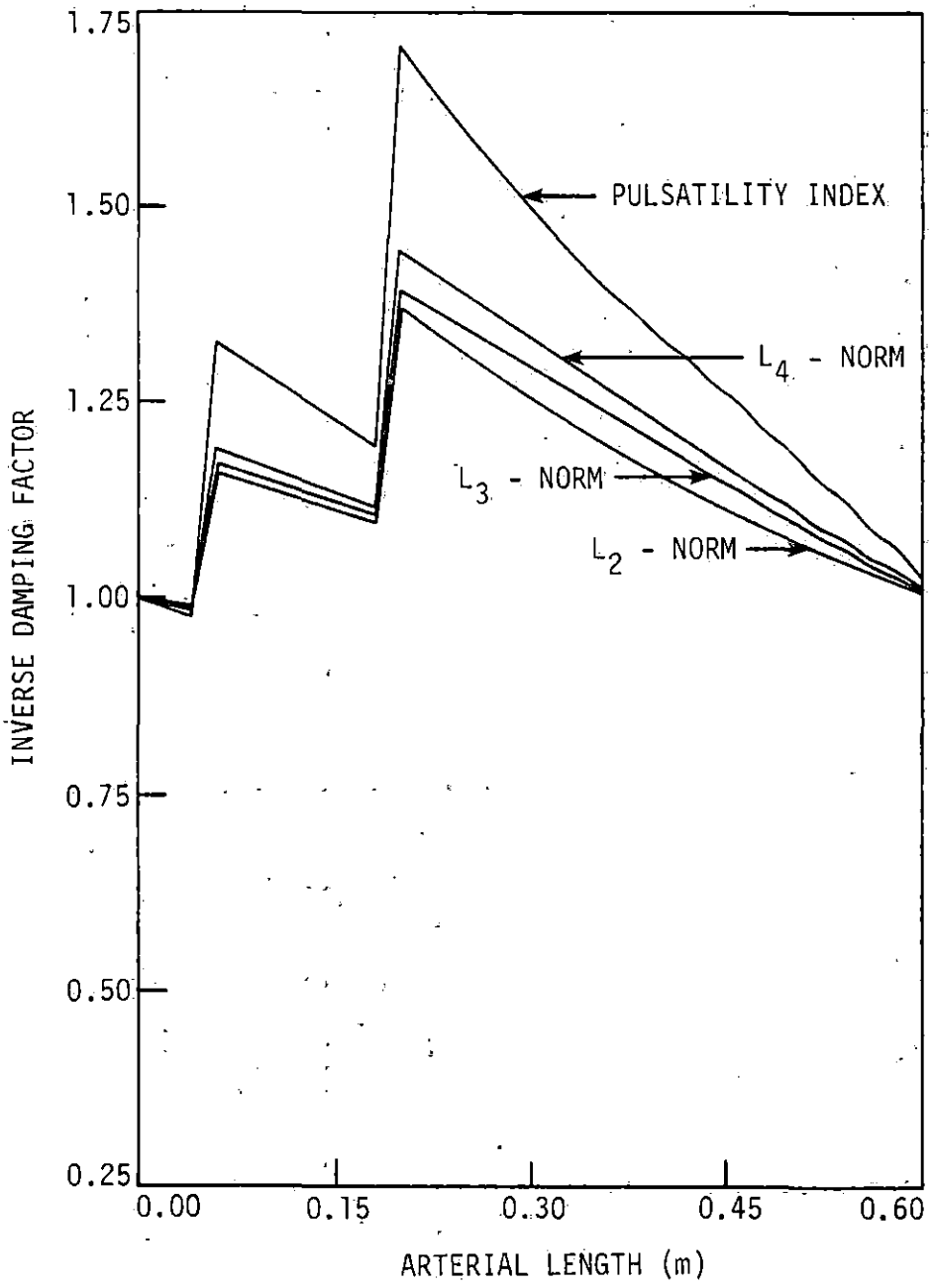

FIGURE 5. Inverse Damping Factors of the Pulsatility Index and the L_n-Norms for the Control Case

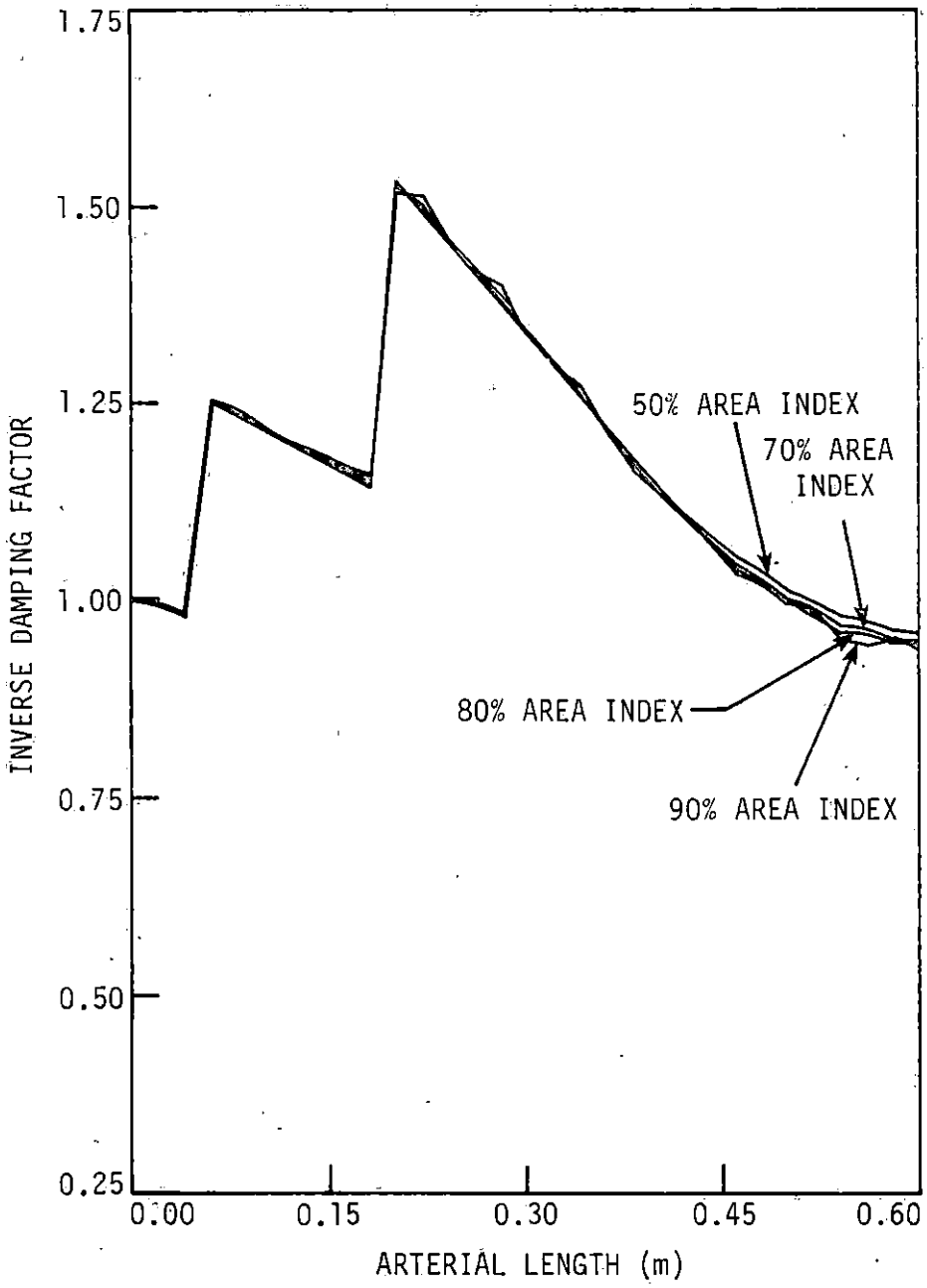

FIGURE 6. Inverse Damping Factors of the Area Indices for the Control Case

did not investigate the effects of elastic taper and possible changes in the state of the peripheral beds on the pressure waveform.

In summary, I concluded that the nonlinear model shows features not present in a linear model, since the convective acceleration term in the momentum equation appears to be a significant factor in determining the pressure pulse wave behavior in both a straight and a tapered elastic tube.

Sensitivity Analysis

With the control case as basis, a sensitivity analysis was conducted by investigating the influences of fluid properties, properties of the arterial wall, branching, and distal resistance on the different general pulsatility indices.

Changes in the blood density by 1% did not bring about significant changes in the PIs. Similarly, setting the blood viscosity to 0, thereby neglecting the friction term in the momentum equation, also had no significant effect. However, an increase of viscosity to $1.2\ 10^{-2}$ Ns/m^2, which corresponds to a hematocrit of 70%, dampened the curves of the PIs and brought them close to values indicative of pathological situations.

The values of E_p, the pressure strain modulus, given in Mozersky et al. (1972) served as primary data to study the influence of properties of the arterial wall. For this simulation, an approximation of (6) by the second order Taylor polynomial was used as an equation of state. The changes in the value of E_p reflect the variations in stiffness of

the arterial wall. For the E_p values of three different age groups, the corresponding PI curves show only slight differences and fall well into the range considered to be normal. Therefore, the stiffness of arterial walls seems to be only of minor importance in determining the PI behavior.

To assess the effects of branches, I simulated the occlusion of both model branches by increasing the four resistance values ten times. Naturally, the steep rise occurring at the branching points in the control case disappeared, but at the same time the rate of decrease along normal arterial section was reduced. However, the drop in the IDF values was large enough to bring the curve of the pulsatility index below the threshold of 0.67 which is correlated with the occurrence of stenotic obstructions. Therefore, low IDF values can also be indicative of reduced blood flow through the branches.

Changes in the distal resistance by factors of 2 and 0.5 brought about significant variations in the PIs, but did not shift the curves to low values that might be correlated with pathological situations. Doubling the distal peripheral resistance resulted in very large rises of the IDF across the two branching points and also in increased curve slopes. Decreasing the peripheral resistance to half the value of the control case diminishes the step size of the IDF across the branching points and also diminishes the curve slopes.

Another point of interest is the behavior of the IDFs close to the distal end. In a clinical environment, the measurement sites for the flow waveform might not be anatomically identical for all patients.

Therefore, dislocating the probe by several centimeters should not result in significantly different measurements if the IDF method is to be of practical value. Except for the case of an increased peripheral resistance, the rate of change in the distal region, away from branches, is small enough so that results obtained at two locations only centimeters apart correlate very closely.

Stenosed Arteries

To investigate the effect of obstructions, stenoses with different degrees of occlusion were placed into the main artery 0.4m from the iliac bifurcation.

Figures 7 to 10 show the results for the case of an obstruction which provides a 90% lumen area reduction. A large pressure drop occurs across the stenosis, so that the distal pressure is very low. Also, the flow waveform distal to the stenosis is dampened and does not exhibit a phase of flow reversal. The IDFs for the pulsatility index and the L_n-norms drop very suddenly in the vicinity of the stenosis and stay approximately constant downstream of the stenosis. Also, the IDFs for the area indices are shifted to lower values and differ significantly from the control case.

In summary, the hemodynamic effects of a 90% stenosis are severe and recognizable in the IDFs of all pulsatility indices considered. Therefore, a diagnosis of stenotic obstructions seems to be feasible for a severely occluded artery.

A less severe stenosis was considered next. Figures 11 to 14

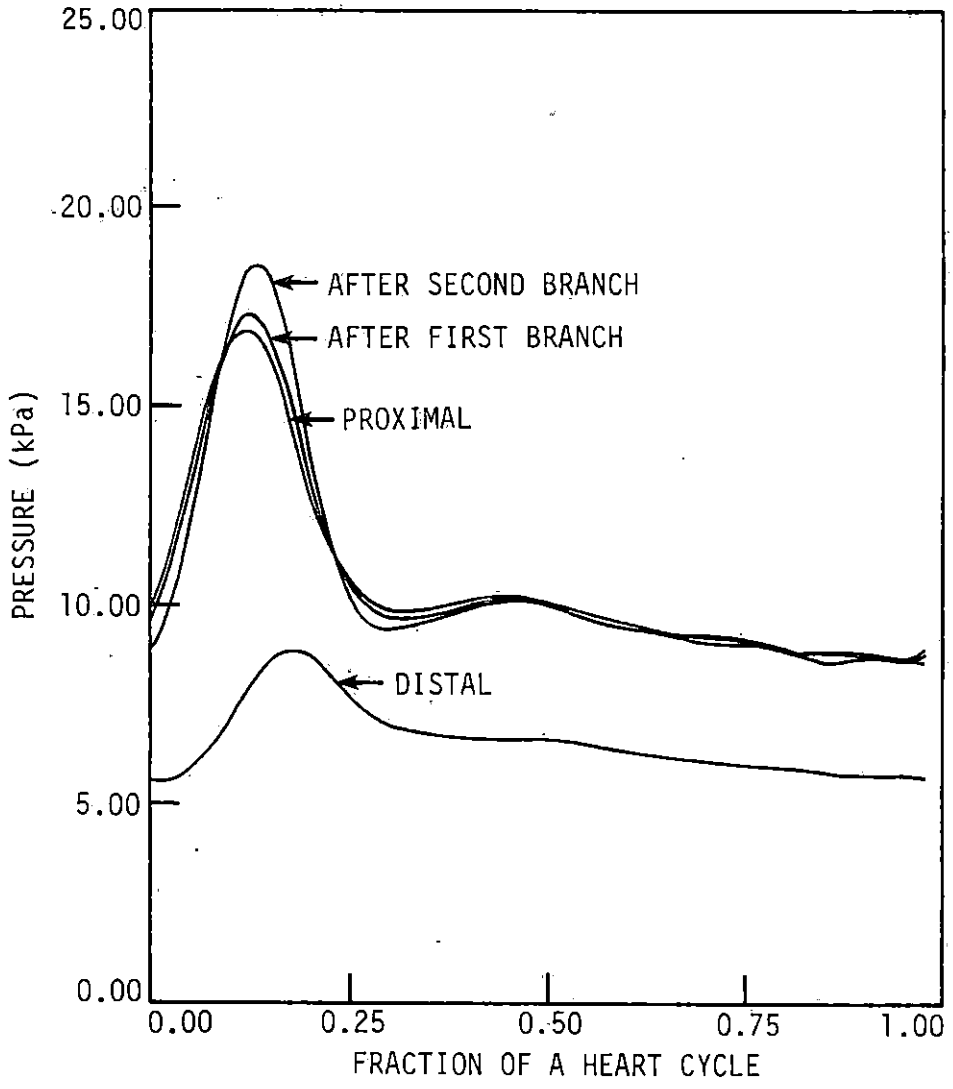

FIGURE 7. Pressure Waves along the Artery for a 90% Stenosis

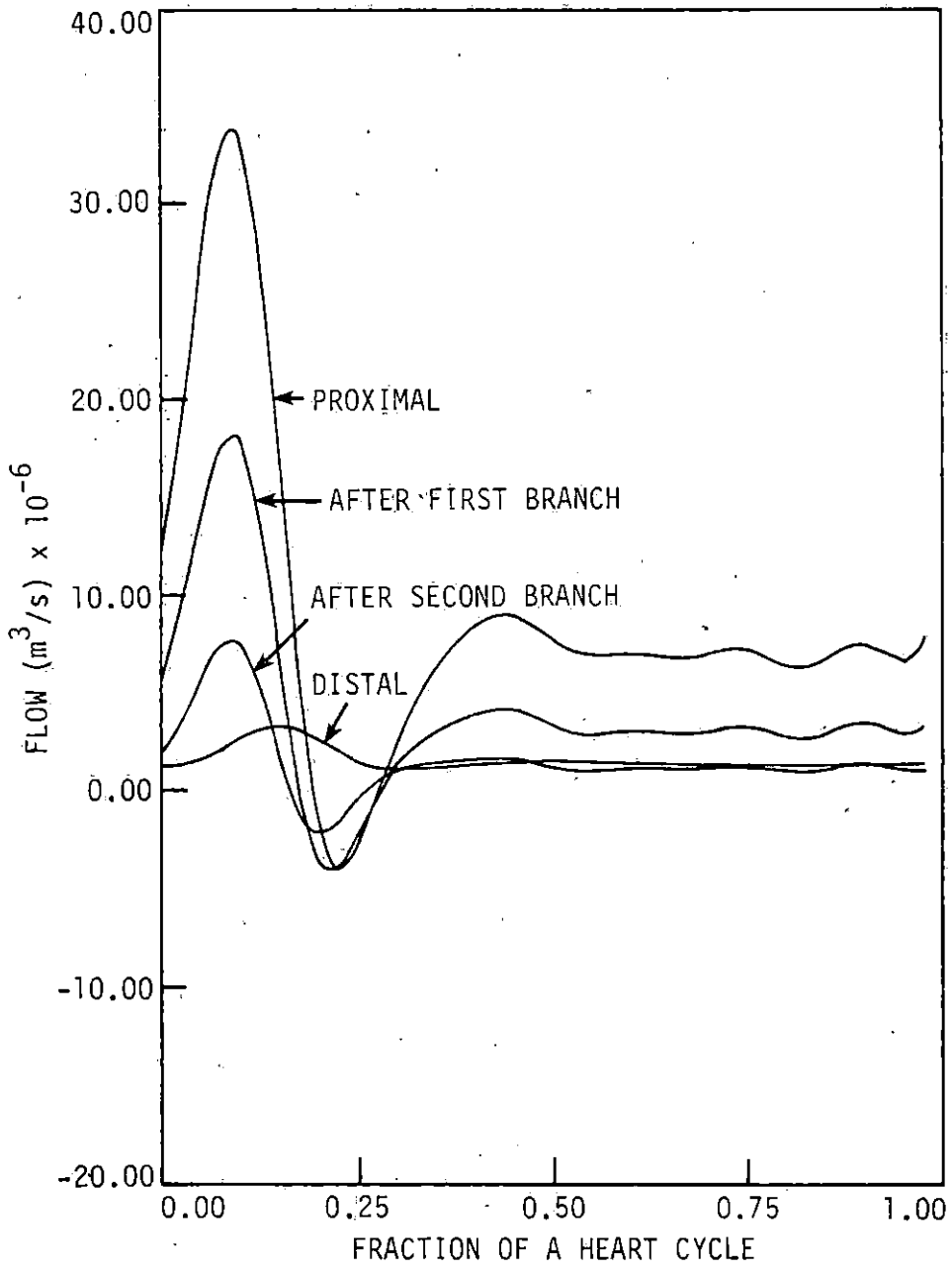

FIGURE 8. Flow Waves along the Artery for a 90% Stenosis

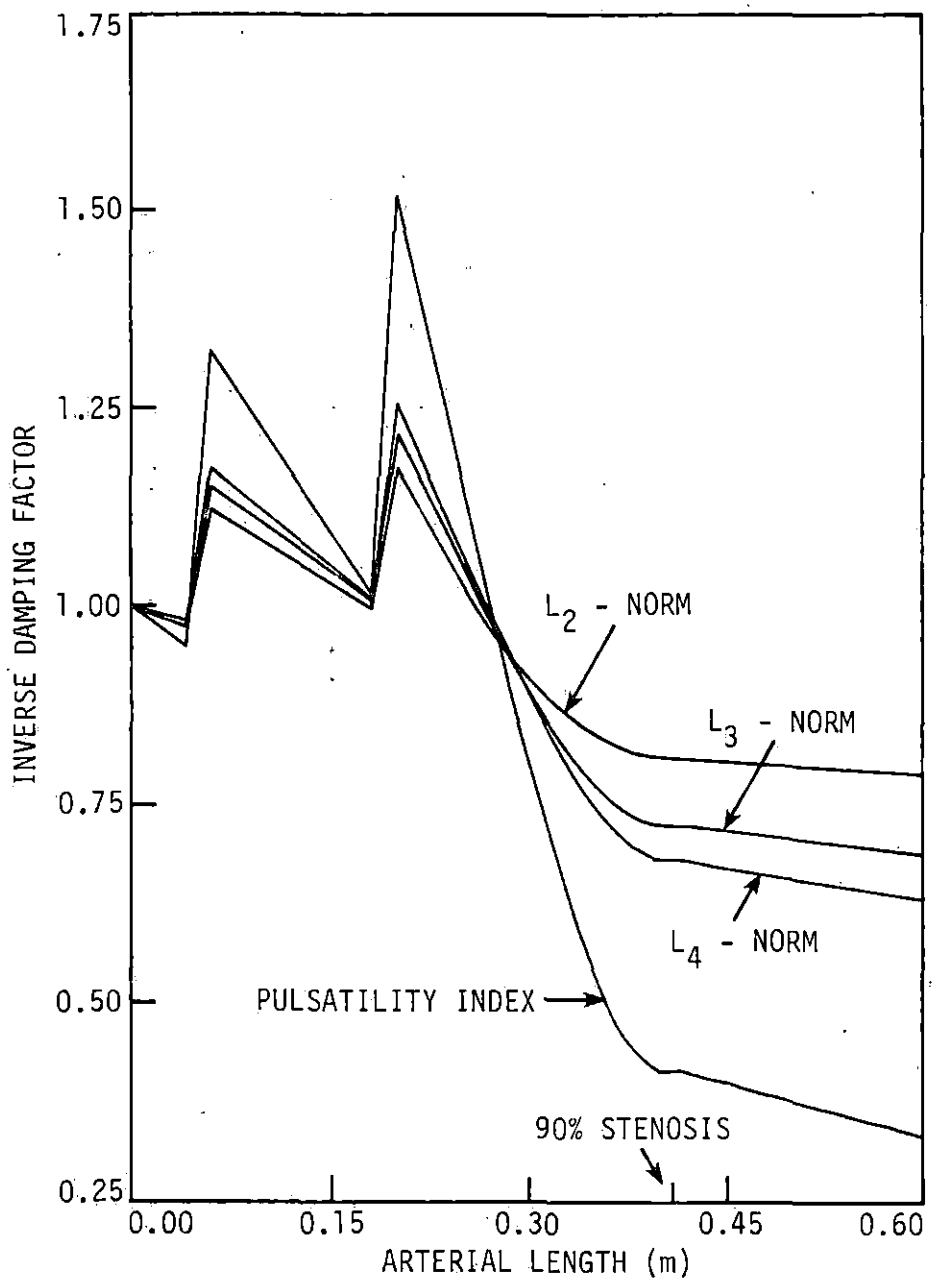

FIGURE 9. Inverse Damping Factors of the Pulsatility Index and the L_n-Norms for a 90% Stenosis

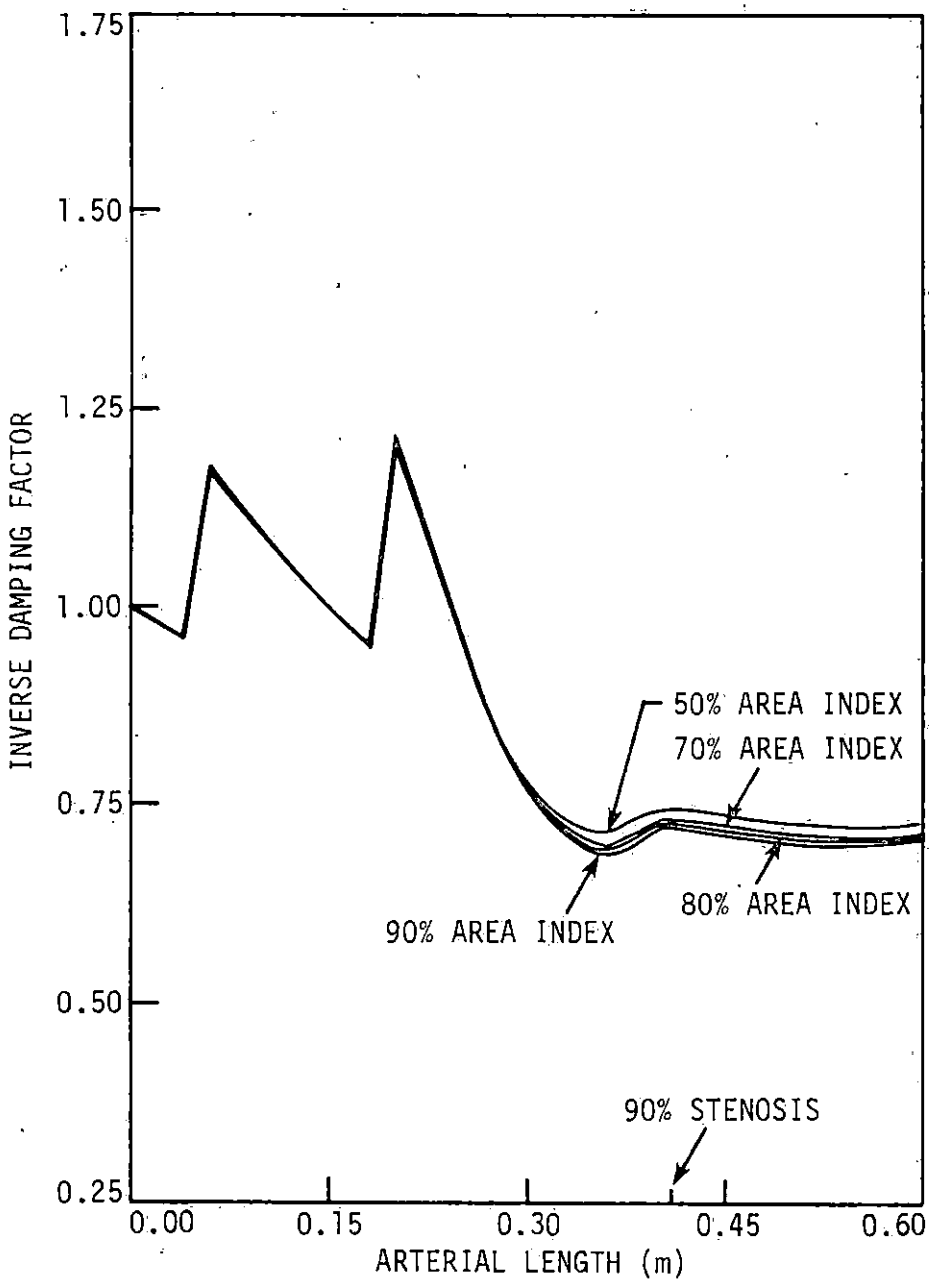

FIGURE 10. Inverse Damping Factors of the Area Indices for a 90% Stenosis

contain the data curves obtained for a 75% stenosis. Still, the distal pressure is reduced, and the distal flow wave is dampened, but compared to the 90% stenosis, these effects are less pronounced. The drop in the IDF of the pulsatility index is also present; however, it takes place more slowly and continues also after the stenosis location. Therefore, different results will be obtained at different measurement sites downstream of the stenosis. The more distal from the stenosis the waveform is evaluated, the more indicative of an obstruction it will be.

Thus, from the model results it follows that less severe stenoses are best detected if the distal PI measurement is taken at some distance distal from the stenosis. Moreover it is important that measurements are not taken in the vicinity of branches since big fluctuation of the PI occur around branches. For practical purposes, these two requirements are probably hard to meet, as the exact location of stenosis and branches are generally not known.

Evans et al. (1980) indicate that in experimental animals the state of the peripheral beds play an important role in determining the IDF for nonsevere stenoses (<86%). To clarify this point, I placed a 50% stenosis into my model and let the resistances of the peripheral bed vary by a factor of 2. For an increased peripheral resistance, the IDF curves remain above 1, and are not significantly different from curves without a stenosis. However, if the distal resistance was decreased, the drop in the IDF was large enough to bring the IDF of the PI below 0.67 at the distal end. A stenosis would then be diagnosed correctly. Thus, an high peripheral resistance tends to cover the effects of

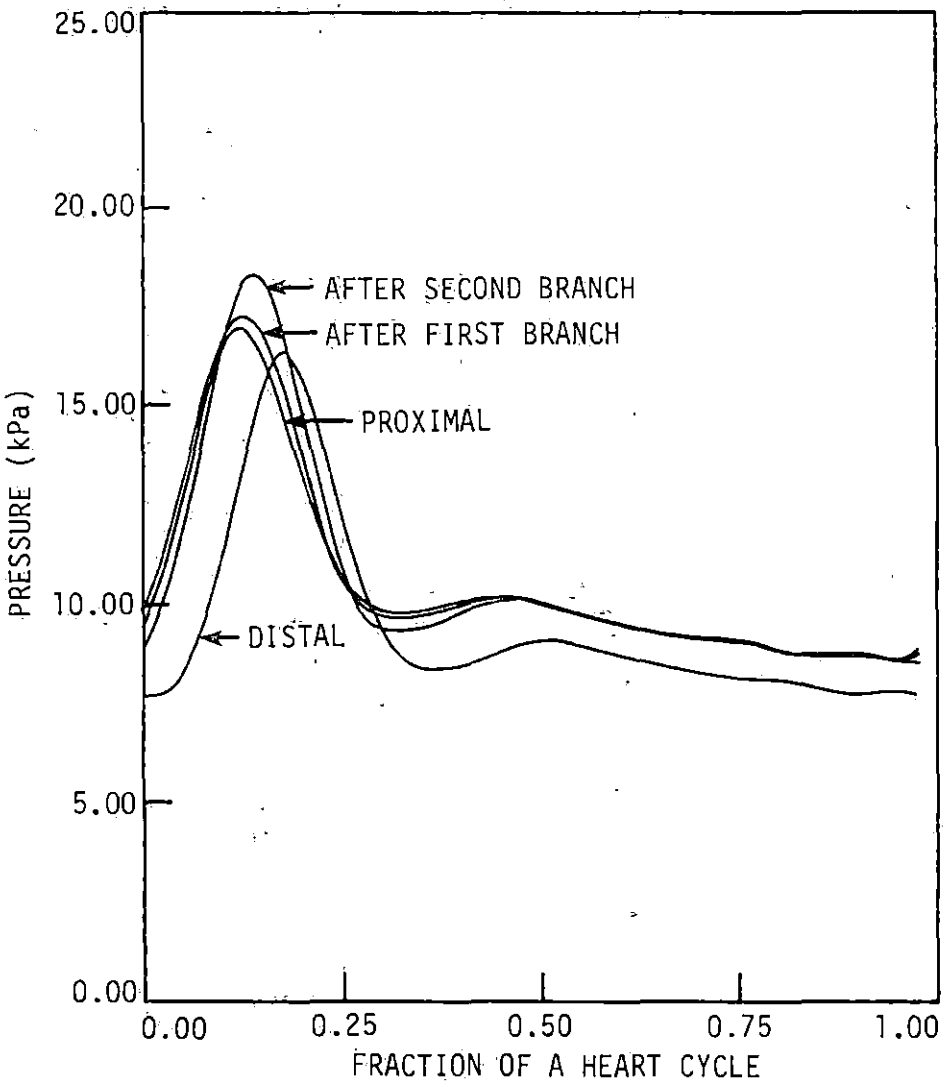

FIGURE 11. Pressure Waves along the Artery for a 75% Stenosis

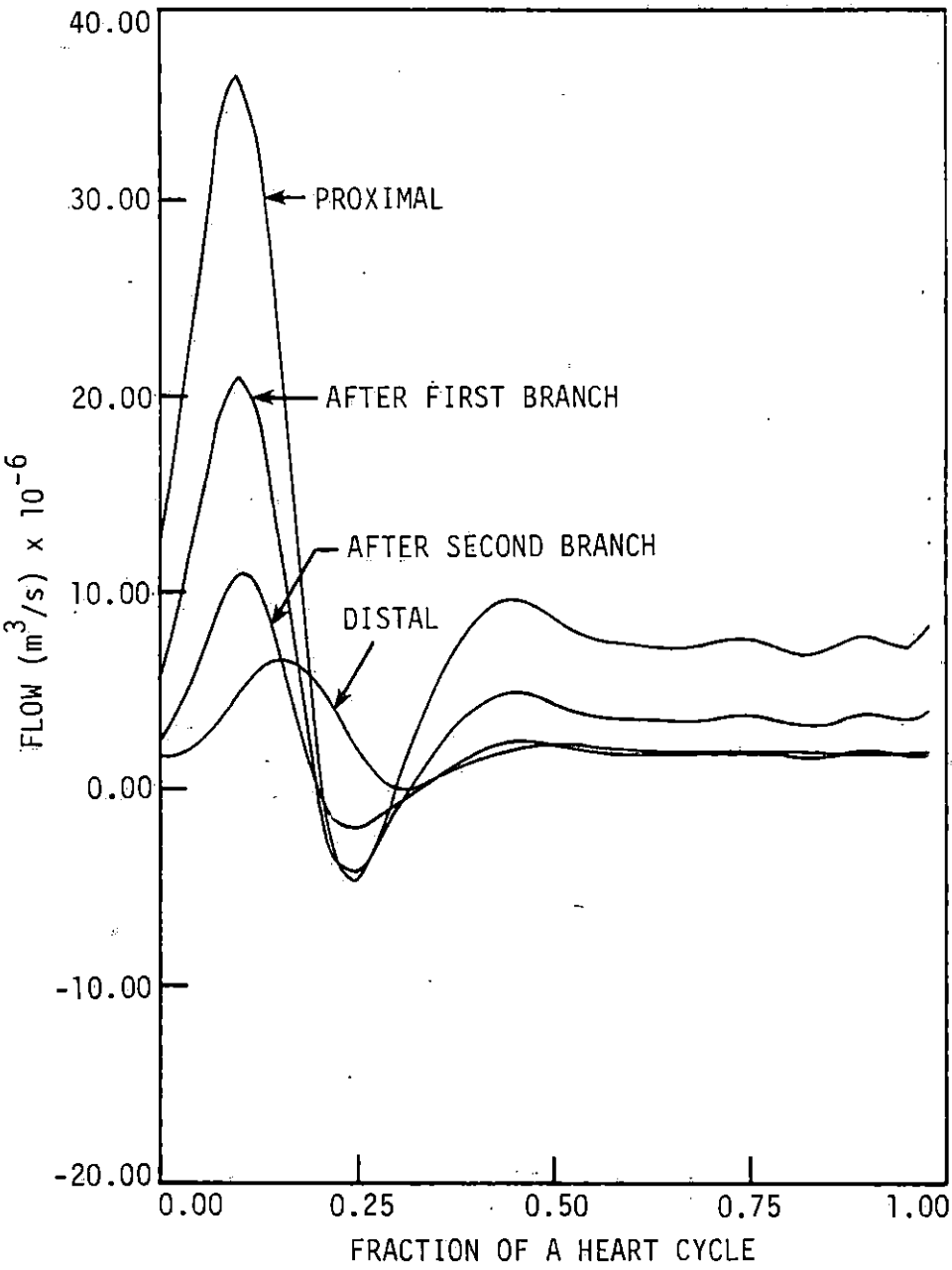

FIGURE 12. Flow Waves along the Artery for a 75% Stenosis

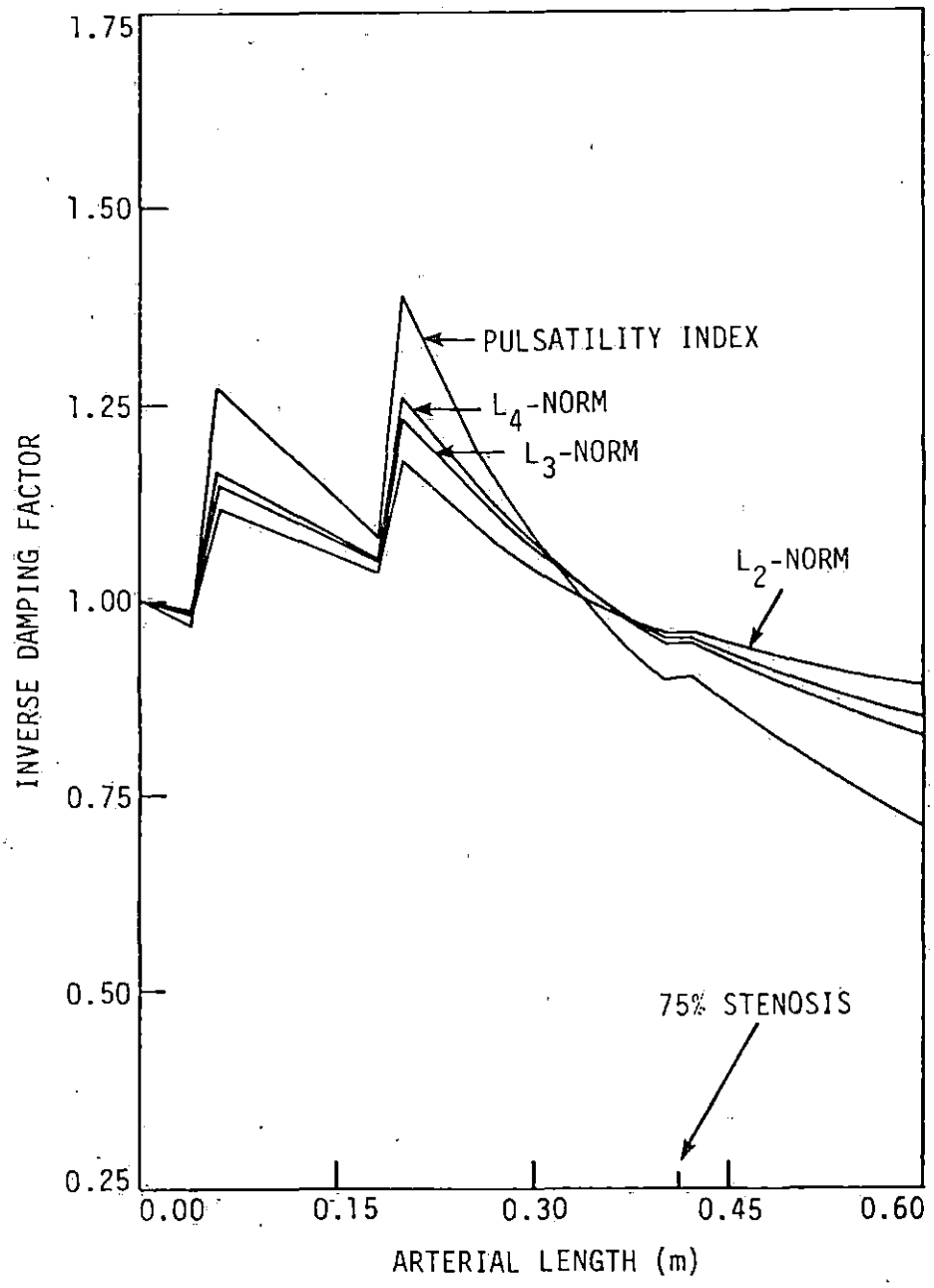

FIGURE 13. Inverse Damping Factors of the Pulsatility Index and the L_n-Norms for a 75% Stenosis

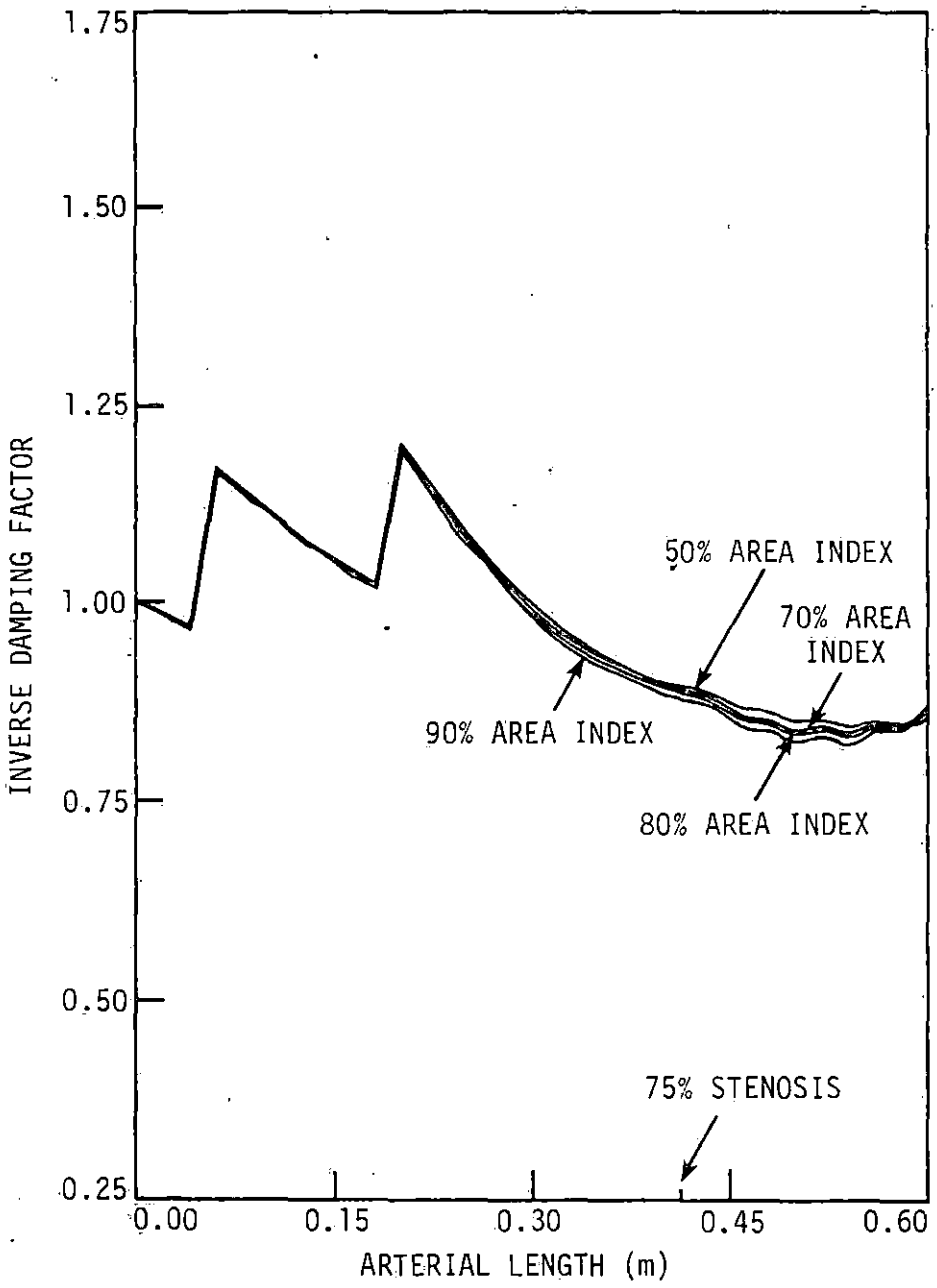

FIGURE 14. Inverse Damping Factors of the Area Indices for a 75% Stenosis

stenoses which are not severly constricting the arterial lumen.

From the model results, I concluded that (1) a low peripheral resistance is essential to allow the diagnosis of less severe stenoses with the PI method, and (2) the eight general pulsatility indices in all situations show the same qualitative behavior, with the pulsatility index being the most sensitive index. Therefore, in a diagnostic method it should be sufficient to concentrate on the behavior of the pulsatility index.

SUMMARY AND CONCLUSION

A model of blood flow in the arteries of the human leg has been developed based on three equations: the continuity equation, the momentum equation, and an equation of state. The model geometry together with the system parameters in the control case were taken from Raines et al. (1974). Because of the nonhomogeneous model geometry, the finite element method was used to solve the nonlinear model equations on a high-speed digital computer.

A comparison of the nonlinear model and a corresponding linear model showed that the nonlinear convective acceleration term in the momentum equation causes significant changes in the solution for both straight and tapered elastic vessels, and therefore should not be neglected.

Eight dimensionless quantities called general pulsatility indices were associated with the flow waveform and investigated in this study: the conventional pulsatility index, the L_2, L_3, and L_4 norms, and the 50%, 70%, 80%, and 90% area indices.

A sensitivity analysis conducted to reveal the influences of various system parameters on the pulsatility indices showed that the information contained in the eight indices was equivalent, with the pulsatility index as presently used in the clinical environment being the most sensitive index. Also, from results of the sensitivity analysis, I concluded that a diagnostic method using the pulsatility index is not significantly affected by changes in blood density, by differences in the arterial stiffness likely to be encountered, or by

low values of blood viscosity. However, high blood viscosity, branches, and the condition of the peripheral beds can exhibit a considerable influence.

A simulation of the effects of stenoses with various degrees of severity, and located in the popliteal artery, seems to indicate that severe arterial stenoses (more than 90% area occlusion) can be diagnosed by a method using pulsatility indices if the peripheral beds are in a normal condition. Less severe stenoses are only detected if the peripheral resistance is low.

In summary, a noninvasive method for detecting arterial obstructions using the PI method seems to be feasible if the following guidelines are observed:

1. The measurement site should not be located in the vicinity of a branch.
2. The blood viscosity should be normal or low rather than elevated.
3. The peripheral resistance should be made as low as possible.
4. If possible, the measurements should not be taken close to the stenosis location.

These recommendations are drawn from a computer based study and presently do not have support from clinical studies. Other than an agreement of the pressure and flow curves of the model with physiological findings, I do not have an assessment of how well my model approximates the in vivo situation. Thus, it would be of interest to conduct animal experiments in which all system parameters can be

monitored to verify the validity of the model equations. Also, a clinical study based on my results could be useful in determining if the recommendations given above are of practical use in a clinical setting.

BIBLIOGRAPHY

Baird, R. N., R. J. Lusby, D. R. Bird, A. E. B. Giddings, R. Skidmore, J. P. Woodcock, R. E. Horton, and J. H. Peacock. 1979. Pulsed Doppler angiography in lower limb arterial ischemia. Surgery 86(6):818-825.

Boughner, D. R., and M. R. Roach. 1971. Effect of low frequency vibration on the artery wall. Circ. Res. 29:136-144.

Evans, D. H., W. W. Barrie, M. J. Asher, S. Bentley, and P. R. F. Bell. 1980. The relationship between ultrasonic pulsatility index and proximal arterial stenosis in a canine model. Circ. Res. 46(4):470-475.

Gosling, R. G., G. Dunbar, D. H. King, D. L. Newman, C. D. Side, J. P. Woodcock, D. E. Fitzgerald, J. S. Keates, and D. MacMillan. 1971. The quantitative analysis of occlusive peripheral arterial disease by a non-intrusive ultrasonic technique. Angiology 22:52-55.

Gosling, R. G., and D. H. King. 1974. Continuous wave ultrasound as an alternative and complement to x-rays in vascular examinations. Pages 266-282 in R. S. Reneman, ed. Cardiovascular applications of ultrasound. Am. Elsevier Publications, Inc., New York.

Harris, P. L., L. A. Taylor, F. D. Cave, and D. Charlesworth. 1974. The relationship between Doppler ultrasound assessment and angiography in occlusive arterial disease of the lower limbs. Surg. Gynecol. Obstet. 138:911-914.

Johnston, K. W., and I. Taraschuk. 1976. Validation of the role of pulsatility index in quantitation of the severity of peripheral arterial occlusive disease. Am. J. Surg. 131:295-297.

Johnston, K. W., B. C. Maruzzo, and R. S. C. Cobbold. 1977. Errors and artifacts of Doppler flowmeters and their solution. Arch. Surg. 112:1335-1342.

Johnston, K. W., B. C. Maruzzo, and R. S. C. Cobbold. 1978. Doppler methods for quantitative measurement and localization of peripheral arterial occlusive disease by analysis of the blood flow velocity waveform. Ultrasound in Med. & Biol. 4:209-223.

Lee, B. Y., F. S. Trainor, W. R. Thoden, D. Kavner, and J. L. Madden. 1980. Use of noninvasive electromagnetic flowmetry in the assessment of peripheral arterial disease. Surg. Gynecol. Obstet. 150:342-346.

McDonald, D. A. 1974. Blood flow in arteries. 2nd ed. The Williams & Wilkins Company, Baltimore.

Mozersky, D. J., D. S. Sumner, D. E. Hokanson, and D. E. Strandness, Jr. 1972. Transcutaneous measurement of the elastic properties of the human femoral artery. Circulation 46:948-955.

Raines, J. K., M. Y. Jaffrin, and A. H. Shapiro. 1974. A computer simulation of arterial dynamics in the human leg. J. Biomechanics 7:77-91.

Remington, J. W., and E. H. Wood. 1956. Formation of peripheral pulse contour in man. J. Appl. Physiol. 9:433-442.

Roach, M. R., and A. C. Burton. 1959. The effect of age on the elasticity of human iliac arteries. Can. J. Biochem. Physiol. 37:557-570.

Rooz, E. 1980. A finite-element simulation of pulsatile flow in flexible tubes. Ph.D. Thesis. Iowa State University.

Schaaf, B. W., and P. H. Abbrecht. 1972. Digital computer simulation of human systemic arterial pulse wave transmission: a nonlinear model. J. Biomechanics 5:345-364.

Snyder, M. F., V. C. Rideout, and R. J. Hillestad. 1968. Computer modeling of the human arterial tree. J. Biomechanics 1:341-353.

Streeter, V. L., W. F. Keitzer, and D. F. Bohr. 1963. Pulsatile pressure and flow through distensible vessels. Circ. Res. 13:3-20.

U.S. Department of Health and Human Services. 1980. National heart, lung, and blood institute's fact book for fiscal year 1980. NIH Publication No. 81-2105.

U.S. Department of Health, Education, and Welfare. 1979. Seventh report of the director, national heart, lung, and blood institute. NIH Publication No. 80-1672.

Wemple, R. R., and L. F. Mockros. 1972. Pressure and flow in the systemic arterial tree. J. Biomechanics 5:629-641.

Westerhof, N., F. Bosman, C. J. de Vries, and A. Noordergraaf. 1969. Analog studies of the human systemic arterial tree. J. Biomechanics 2:121-143.

Womersley, J. R. 1957. An elastic tube theory of pulse transmission and oscillatory flow in mammalian arteries. Wright Air Development Center Technical Report TR 56-614.

Woodcock, J. P., R. G. Gosling, and D. E. Fitzgerald. 1972. A new non-invasive technique for assessment of superficial femoral artery obstruction. Br. J. Surg. 59(3):226-231.

Young, D. F., and F. Y. Tsai. 1973. Flow characteristics in models of arterial stenosis-II. unsteady flow. J. Biomechanics 6:547-559.

Young, D. F. 1979. Fluid mechanics of arterial stenoses. J. Biomech. Eng. 101:157-175.

ACKNOWLEDGEMENTS

The present thesis would not have been possible without the gentle guidance and the unlimited support that I received from my heavenly Father, from the Lord Jesus Christ, and from the Holy Spirit, who filled my often doubtful heart with optimism, confidence, and endurance. Also invaluable was the patience and the tutorship of Professor D. F. Young, who introduced me to the fascinating field of hemodynamics and provided me with optimal working conditions. Moreover, he edited this thesis and eliminated numerous idiomatic expressions bearing a quite noticeable resemblance to Austrian idioms. I am grateful to Professors T. R. Rogge and R. C. Seagrave for serving on my committee. Finally, I would like to thank the Austrian-American Fulbright Commission and the Lewis G. Smith Trust of Philadelphia for providing part of my financial support.

APPENDIX

This appendix details the element equations obtained by applying the Galerkin method to the partial differential equations simulating three different flow situations: An arterial section without a branch, an arterial section with a branch, and a stenosed arterial section. The element representation has the form

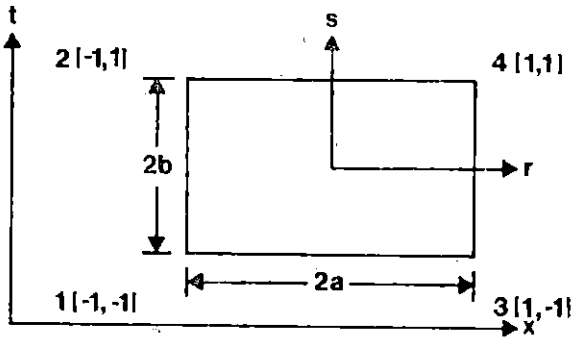

giving the following relations:

$$Q(r,s) = [N(r,s)]\{q\}$$

$$p(r,s) = [N(r,s)]\{p\}$$

where

$$\{q\} = [q_1, q_2, q_3, q_4]^T$$

$$\{p\} = [p_1, p_2, p_3, p_4]^T$$

$$[N(r,s)] = (1/4)[(1-r)(1-s), (1-r)(1+s), (1+r)(1-s), (1+r)(1+s)]$$

The vectors {p} and {q} contain the values of pressure and flow at the four element nodes. [N(r,s)] is the shape function vector in its dimensionless form resulting from a transformation of the (x,t) coordinates to the (r,s) coordinates to facilitate the integration step included in the Galerkin method.

If the values of pressure and flow at node 1 and 3 are assumed to be known, only two algebraic equations have to be formed for each partial differential equation. Therefore, it is sufficient to multiply the differential forms by only two shape functions. For this step, I arbitrarily chose to include the two shape functions corresponding to node 2 and 4:

$$[N]^R = [(1-r)(1+s),\ (1+r)(1+s)]^T$$

For a normal arterial section without a branch, the Galerkin method applied to equations (7) and (10) yields in its dimensionless form with the reduced multiplication factor

$$\int\int [N]^R([N]_r\{q\} + C_0[N]_s\{p\} + C_1[N]\{p\}[N]_s\{p\})\ a\ b\ dr\ ds = 0$$

and

$$\int\int [N]^R(A[N]_s\{q\} + 2[N]\{q\}[N]_r\{q\} - (1/A)[N]\{q\}[N]\{q\}\frac{\partial A}{\partial r} +$$

$$+ (A^2/\rho)[N]_r\{p\} + \frac{8\pi\mu}{\rho}[N]\{q\})\ a\ b\ dr\ ds = 0$$

where $[N]_x$ indicates the differentiation of [N] with respect to x (x = r,s).

For notational convenience used throughout the appendix, the equations are multiplied by 18 and then integrated term by term. For the continuity equation the three terms evaluate as

$$\int\int [N]^R[N]_r\{q\}\ a\ b\ dr\ ds = b \begin{bmatrix} -3 & -6 & 3 & 6 \\ & & & \\ -3 & -6 & 3 & 6 \end{bmatrix} \{q\}$$

$$\int\int [N]^R C_0 [N]_s \{p\}\ a\ b\ dr\ ds = (C_0 a) \begin{bmatrix} -6 & 6 & -3 & 3 \\ -3 & 3 & -6 & 6 \end{bmatrix} \{p\}$$

$$\int\int [N]^R C_1 [N]\{p\}[N]_s \{p\}\ a\ b\ dr\ ds = (C_1 a/2)\ B\{p\}$$

where $B = (b_{ij})$ is given by

$$b_{11} = -3p_1 + 3p_2 - p_3 + p_4$$

$$b_{12} = -6p_1 + 6p_2 - 2p_3 + 2p_4$$

$$b_{13} = -p_1 + p_2 - p_3 + p_4$$

$$b_{14} = -2p_1 + 2p_2 - 2p_3 + 2p_4$$

$$b_{21} = -p_1 + p_2 - p_3 + p_4$$

$$b_{22} = -2p_1 + 2p_2 - 2p_3 + 2p_4$$

$$b_{23} = -p_1 + p_2 - 3p_3 + 3p_4$$

$$b_{24} = -2p_1 + 2p_2 - 6p_3 + 6p_4$$

For the momentum equation, only the three terms that cannot be derived by analogy from terms appearing in the continuity equation will be listed below.

$$\int\int [N]^R 2 [N]\{q\}[N]_r \{q\}\ a\ b\ dr\ ds = b\ B'\{q\}$$

where $B' = (b_{ij})$ is given by

$$b_{11} = -2q_1 - 2q_2 + 2q_3 + 2q_4$$

$$b_{12} = -2q_1 - 6q_2 + 2q_3 + 2q_4$$

$$b_{13} = -q_1 - q_2 + q_3 + q_4$$

$$b_{14} = -q_1 - 3q_2 + q_3 + 3q_4$$

$$b_{21} = -q_1 - q_2 + q_3 + q_4$$

$$b_{22} = -q_1 - 3q_2 + q_3 + 3q_4$$

$$b_{23} = -2q_1 - 2q_2 + 2q_3 + 2q_4$$

$$b_{24} = -2q_1 - 6q_2 + 2q_3 + 6q_4$$

$$\iint [N]^R (1/A)[N]\{q\}[N]\{q\}\frac{\partial A}{\partial r}\, a\, b\, dr\, ds = (Kab/2)\, B''\{q\}$$

where K is a factor arising from the application of the mean value theorem of integral calculus to the two factors involving the area A. Thus, the very tedious integration over the area is avoided. The matrix $B'' = (b_{ij})$ is given by

$$b_{11} = 3q_1 + 3q_2 + q_3 + q_4$$

$$b_{12} = 3q_1 + 9q_2 + q_3 + 3q_4$$

$$b_{13} = q_1 + q_2 + q_3 + q_4$$

$$b_{14} = q_1 + 3q_2 + q_3 + 3q_4$$

$$b_{21} = q_1 + q_2 + q_3 + q_4$$

$$b_{22} = q_1 + 3q_2 + q_3 + 3q_4$$

$$b_{23} = q_1 + q_2 + 3q_3 + 3q_4$$

$$b_{24} = q_1 + 3q_2 + 3q_3 + 9q_4$$

$$\int\int [N]^R \left(\frac{8\pi\mu}{\rho}\right)[N]\{q\}\ a\ b\ dr\ ds = K' \begin{bmatrix} 4 & 8 & 2 & 4 \\ 2 & 4 & 4 & 8 \end{bmatrix} \{q\}$$

where $K' = \frac{8\pi\mu}{\rho} ab$.

For an arterial section with a branch, Galerkin's method applied to equations (11) and (12) yields

$$\int\int [N]^R ([N]_r\{p\})\ a\ b\ dr\ ds = 0$$

and

$$\int\int [N]^R (C[N]_s\{p\} - R_1 C[N]_s^B\{q\} + (1/R_1)[N]\{p\} - (1+R_1/R_2)[N]^B\{q\})\ a\ b\ dr\ ds = 0$$

where B, the branch flow, is written in terms of nodal flows as

$$B = [N]^B\{q\}$$

with

$$[N]^B = (1/2)[(1-s),\ (1+s),\ -(1-s),\ -(1+s)]$$

The two terms involving the pressure can be developed by analogy from terms in the normal continuity and momentum equations. The two terms involving the branch flow evaluate as follows

$$\int\int [N]^R R_1 C[N]_s^B\{q\}\ a\ b\ dr\ ds = R_1 Ca \begin{bmatrix} 9 & -9 & -9 & 9 \\ 9 & -9 & -9 & 9 \end{bmatrix} \{q\}$$

$$\int\int [N]^R W[N]^B\{q\}\ a\ b\ dr\ ds = (Wab) \begin{bmatrix} -6 & -12 & 6 & 12 \\ -6 & -12 & 6 & 12 \end{bmatrix} \{q\}$$

where $W = (1+R_1/R_2)$.

At the distal end, the boundary condition for pressure and flow has the same form as the continuity equation for branch flow. Thus, the Galerkin method yields

$$\int (1+s)(C[N]_s^D\{p\} - R_1 C[N]_s^D\{q\} + (1/R_2)[N]^D\{p\} - (1+R_1/R_2)[N]^D\{q\})\, b\, ds = 0$$

where

$$[N]^D = (1/2)[0,\ 0,\ (1-s),\ (1+s)]$$

The integration is straight forward.

For an obstructed arterial section, the differential forms corresponding to equations (13) and (14) are

$$\int\int [N]^R [N]_r\{q\}\, a\, b\, dr\, ds = 0$$

and

$$\int\int [N]^R(-K_1[N]_\Delta\{p\} + K_2[N]\{q\} + K_3[N]\{q\}[N]\{q\} + K_4[N]_s\{q\})\, a\, b\, dr\, ds = 0$$

where

$$[N]_\Delta = (1/2)[(1-s),\ (1+s),\ -(1-s),\ -(1+s)]$$

and K_i, i=1,4, constants for the integration process, are given in detail in equation (14). The matrix for the pressure drop term is

$$\int\int [N]^R K_1 [N]_\Delta\{p\}\, a\, b\, dr\, ds = (K_1 ab) \begin{bmatrix} 6 & 12 & -6 & -12 \\ & & & \\ 6 & 12 & -6 & -12 \end{bmatrix} \{p\}$$